Ab initio thermodynamics of complex alloys: The case of Al- and Mn-doped ferritic steels

Rémy Besson, Jerome Dequeker, Ludovic Thuinet, Alexandre Legris

Ab initio thermodynamics of complex alloys: the case of Al- and Mn-doped ferritic steels

Rémy Besson, Jérôme Dequeker, Ludovic Thuinet, Alexandre Legris

Unité Matériaux Et Transformations (UMET), CNRS UMR 8207,
Université de Lille, 59655 Villeneuve d'Ascq Cedex, France

E-mail: Remy.Besson@univ-lille.fr

Abstract

In the context of Al- and Mn-doped ferritic steels, we progressively elaborate an atomic-scale energy model to reproduce the thermodynamic behavior of quaternary Fe-Al-Mn-C on a bcc lattice. This model is built on physical concepts: DFT calculations, pair Hamiltonians, non-configurational thermal effects, these elements being combined in a reasoned way to lead to a mastered and predictive formulation. In particular, this approach allows to explore the correlation between ordering in substitutional ternary Fe-Al-Mn and interstitial carbon, which brings new elements to the metallurgy of carbon in ferritic steels.

I Introduction

Current economic and ecological policies encourage car manufacturers to limit gas emissions, and reducing the mass of vehicles keeping their robustness and ductility would help to satisfy these criteria. One approach in this direction consists in lightening the materials, especially the steel-made parts. In the automotive sector, the research is mainly concerned with advanced high-strength steels (AHSS). For such multiphase steels, heat treatments are important because they monitor the phase fractions, as well as the chemical composition which plays an important role. In particular, adding manganese increases the proportion of austenite at equilibrium while aluminum stabilizes ferrite while contributing to an important decrease of the density. In the following, we are therefore interested in Fe-Al-Mn-C alloys (with high Fe content).

Considering the iron-rich corner of this quaternary system, our starting point is the iron-aluminum binary system, studied extensively [1-3] for several decades. Its well-known equilibrium phase diagram, determined by experimental techniques, is recalled in the

Supplemental Material (Figure S1). On the iron-rich side, there are three bcc-based compounds: the A2 solid solution, the Fe_3Al ordered compound with $D0_3$ structure, and the FeAl ordered compound with B2 structure. The Fe-Mn phase diagram, also well-known (not displayed for brevity), indicates that the presence of Mn strongly stabilizes the fcc Fe(Mn) solid solution on a large composition and temperature range. The Al-Mn phase diagram contains many stable phases at different compositions, which however are not based on a bcc or an fcc lattice. In the Fe-Al-Mn system based on the bcc lattice, the Fe_2AlMn compound has an $L2_1$ ordered structure below 898 K, then becomes B2 before moving gradually to the A2 solid solution up to 1677 K and finally melting at 1686 K [4]. However, the $L2_1$ compound is not perfectly stoichiometric and its composition can include up to 10% additional iron [4,5]. Turning towards the role of carbon, the Fe-C solid solution was studied using various theoretical approaches that showed that C-C interactions in bcc Fe should be essentially repulsive [6-7]. Similar previous studies were also concerned by the mechanisms underlying the $\alpha \rightarrow \alpha'$ martensitic transformation [8-15]. These studies were mainly devoted to unraveling the complex influence of more or less long-range elasticity-driven C-C interactions on the formation of diluted Fe-C ordered compounds with various orderings of C on octahedral sites. Using various theoretical/simulation approaches, these works revealed persistent uncertainties about the relative stabilities of such compounds, in particular those with compositions $Fe_{16}C$ or $Fe_{16}C_2$, which confirms that the behaviour of C in iron currently remains an intricate issue coupling thermodynamics and elasticity. Since such valuable investigations required input parameters, e.g. long-range C-C binding energies and local relaxations, extracted from atomic-scale simulations, their reliability was restricted somewhat by (i) the limited size of the supercells used in ab initio calculations, and (ii) the quality of the empirical EAM potentials used for larger supercells. Finally, since our study, being not primarily aimed at pursuing these investigations of Fe-C, is more focused on the complementary issue of interactions between C and substitutional elements in steels, it is worth mentioning several simulation works devoted to the study of Fe-Al-C by means of ab initio and Calphad calculations [16-18], were mainly intended to understand the role of the fcc-based κ-Fe_3AlC "kappa" compound in the phase diagram, and a work on Fe-Ni-C [19] focused on the influence of Ni on martensite tetragonality. In spite of these works, the effect of interactions between C

and substitutional elements on thermodynamics and phase diagrams remains largely unknown. It is our aim to bring information on these topics.

Throughout this study, the whole alloy energetics will be described by means of cluster Hamiltonians [20,21] restricted to short-ranged pair interactions, namely referred to as "on-site" or Ising models [22], allowing for each microscopic configuration, i.e. site occupancies, to calculate the associated energy and therefore to explore the configurational thermodynamics of the system, thus providing a convenient tool to compute phase diagrams from atomic-scale modeling [23]. Although it might a priori seem quite strong, our hypothesis of using only pair Hamiltonians benefits from at least two justifications. Firstly, it is made mandatory by the need to maintain tractability when investigating the thermodynamic properties of more or less multicomponent alloys such as Fe-Al-Mn-C, keeping in mind that we wish to ensure that the approach can be extended to chemically even more heavy (quinary, senary,…) systems. Secondly, previous works on binary metallic alloys (Pt-V [24] or Al-Zr. [25]) have shown that reasonable models can be achieved by means of short-range pair interactions. More recently, cluster Hamiltonians were developed [26] for chemically complex bcc-based alloys up to quinary Mo-Nb-Ta-V-W, which required a large amount of DFT calculations, and pointed out that the first- and second-neighbor pair interactions are significant while third-neighbor pair interactions are much weaker.

Even in the absence of multibody interactions, it should be noted that notably increasing the complexity of the topic, could also be taken into account in pair Hamiltonians, which may thus (i) explicitly include magnetic interactions [27,28], (ii) try to account for long-range pair interactions through a mixed character, lying both in real space and in reciprocal space [29-31], or (iii) include composition-dependent cluster interactions [32]. On the whole, the numerous works on this delicate topic clearly lead to conclude that the selection of an appropriate cluster Hamiltonian taking into account these methodological extensions may quickly become complex and even intractable when the number of chemical species increases. In this context, and to maintain tractability in this work on quaternary body-centered Fe-Al-Mn-C, we therefore consider only pair interactions, referred to as effective cluster interactions afterward since the energy coefficients of a cluster Hamiltonian may practically change values if the selected set of interactions is modified (adding pairs of longer range for example).

The choice of the type of Hamiltonian being made, it remains to determine the energy coefficients that best describe the system of interest. To address this point, direct approaches [33] attempted to model the electronic interactions from the Coherent Potential Approximation (CPA) supplemented by the Generalized Perturbation Method (GPM), allowing to provide separately each cluster interaction, while inverse approaches [34] postulated a priori Hamiltonian forms (most often pair Hamiltonians) whose coefficients were adjusted by inverse MC simulations, so as to reproduce the values of the observables measured experimentally by neutron and/or X-ray diffraction and/or diffuse scattering. Since the 1990s, with the rise of electronic structure calculations using Density Functional Theory (DFT) [35,36], the energy coefficients have been more and more widely determined by least-squares fit on energies calculated from DFT for a number of atomic structures, referred to as the adjustment structure database (ASDB) in the following. This ab initio-based inverse approach has become extremely popular [37] since the years 2000, probably because of its wide availability and very low cost compared to that of experimental methods, and is thus adopted in the present work. In this context, being interested particularly in the iron-rich part of the system, we adjust the coefficients on the calculated energies of supercells containing significant amounts of Fe, while preserving a moderate size for the ASDB. Together with short-ranged pair interactions, the latter choice constitutes the second central hypothesis underlying our work, the validity of which will also be checked by its ultimate consequences on phase diagrams.

Having established a Hamiltonian to describe the energetics of the system, it is a key-issue to test its thermodynamic validity by obtaining, by means of statistical physics methods, the values of physical observables and comparing them to their counterpart known from experiments and/or other kinds of modelings. This is the essential difference between the approach developed here and those used in more phenomenological (e.g. Calphad-type) methodologies. Our modeling deals only with energy coefficients of cluster Hamiltonians, and the free energy (and therefore the thermodynamic quantities) are then deduced from it without any further adjustable parameters. The accuracy of our results also depends on the choice made to evaluate the entropy. In this work, we resort to three levels of approximation: the “Bragg-Williams”

point mean-field (PMF) approximation, the CVM method (in the tetrahedron approximation) and exact MC simulations.

This work is organized as follows. The methodology is detailed in section II, which deals with the expression of the energy model (cluster Hamiltonian), its relations with the ab initio data and thermodynamic application. The results (section III) are gathered by subsystems with growing chemical complexity. We first investigate the Fe-Al binary alloy, by determining the influence of the pair interaction range and of the ASDB. Effective temperature-dependent energy coefficients are introduced in order to take into account non-configurational effects (phonons…). The role of manganese is then modeled to study the Fe-Al-Mn ternary system, focusing on the influence of the ASDB and on temperature effects. Finally, providing the connection with ferritic steels, the results for Fe-Al-Mn-C are presented. Two models are proposed for this quaternary system: the first one is an extension of ternary models with interactions between interstitial and substitutional sites only, while the second one more realistically considers interactions among interstitial sites.

II Methods

II-1 Choice of cluster Hamiltonians

The Hamiltonian used to describe the energy of the system has the general form [20,21]:

$$H = \sum_{\alpha} J_{\alpha} \sigma_{\alpha} \qquad (1)$$

with σ_{α} the so-called cluster occupation numbers, J_{α} the cluster interactions and α an n-dimensional index referring both to sites and species. We show below that most of the physics contained on the Fe-rich side of the ternary Fe-Al-Mn bcc-based phase diagram can be captured by limiting pair interactions to second neighbors, and that such second-neighbor models offer a sound basis for investigating carbon in ferritic steels. To take into account the free energy associated to phonons, T-dependent effective cluster interactions will also be introduced [38].

II-2 Ab initio calculations

The ab initio calculations were performed using the VASP Package [39,40] with the PAW-PBE approximation [41,42]. Particular care was taken to determine the k-point

mesh grid and cut-off energy for the plane-wave development of the pseudo-wave function. A convergence energy criterion of less than 1 meV/atom was used to determine the optimal values of the parameters, i.e. a 20x20x20 k-point grid for a cubic bcc cell containing two Fe atoms and a 500 eV cut-off energy. All calculations included ion as well as supercell relaxations, and were performed with the standard choice $\mu_{Fe}(init) = 2.2\ \mu_B$ for initial Fe magnetic moments, leading in all cases to final μ_{Fe} close to this value.

A large part of the ASDB configurations corresponded as clusters of solutes embedded in a bcc Fe supercell. In these cases, the relevant quantity was the so-called "grand canonical" substitution (resp. insertion) energy defined as $E^{GC} = E^{SC} - E^{Fe}$, with E^{SC} the energy of the supercell containing Al and/or Mn in substitution (resp. C in insertion) and E^{Fe} the energy of a pure iron supercell with same size. To determine the maximum size of the supercell for these situations, it was necessary to balance resource consumption and non-interaction of solute atoms with periodic images. On the whole, based on considerations described in more detail in the Supplemental Material (Figure S2), the ASDB was thus built using 4x4x4 supercells, unless explicitly mentioned.

II-3 Methodology for phonons and magnons

Knowing the phonon spectrum for each ASDB configuration allows to include in the cluster Hamiltonian vibrational contributions reflecting non-configurational temperature effects. Phonons characterize the vibrations of atoms around their equilibrium positions and were here calculated at the Γ point (the center of the Brillouin zone), which was sufficient to get a good estimate of vibrational contributions to ASDB free energies for the supercell size (N=4) used in this work [43]. Since the lattice parameter that minimizes the free energy of the system depends on temperature (thermal expansion), it would be necessary, in order to refine the thermodynamic description of the system at zero pressure, to calculate phonon frequencies for different lattice parameters and take those values that minimize the vibration free energy, which constitutes the quasi-harmonic approximation. However, this kind of study has shown [44] that even at relatively elevated temperature (800 K) the free energy difference between the harmonic (adopted in this work and that consists in calculating F_{vib} at fixed volume) and quasi-harmonic approximation is only a few meV/atom, a degree of refinement of second

order with respect to other uncertainties in the ab initio input data. We therefore opted to work at constant lattice parameter (the 0 K equilibrium value) to preserve computational resources. The force constants related to phonon frequencies were calculated by the displacement method, which consists in moving each atom in turn by a small increment +/-x= 0.015 Å and +/-2x, and allows to calculate the corresponding Hessian matrix of second derivatives of the energy with respect to atomic positions. From the eigenfrequencies (eigenvalues of the dynamic matrix), the vibration contribution to the configuration free energy of each ASDB member is given by [45]:

$$F_{vib} = k_B T \sum_{q,j} \ln\left[2 \sinh \frac{\hbar \omega_j(q)}{2 k_B T}\right] \qquad (2)$$

For a given T, this contribution is added to the energy of each configuration in the ASDB, which gives rise to temperature-dependent energy coefficients $J_\alpha(T)$ in equation (1).

The effect of magnetic degrees of freedom has been more or less explicitly taken into account by a number of authors, especially in the Fe-Al system [27,28]. At sufficiently low temperatures, a first approach consists in assuming that all magnetic moments of iron (and Mn) atoms are collinear, which has been confirmed by DFT calculations in bcc-based Fe alloys. The low-temperature fluctuations of magnetic moments are well described in the magnon treatment of the Heisenberg model. In this approach, the key-parameter is the exchange integral J_{mag} between nearest-neighbor spins, which was obtained from DFT. For the A2, B32 and $D0_3$ compounds, these calculated values lie between 120 and 200 meV whereas the expected value should be close to 40 meV [27] according to the experimental Curie temperature of pure bcc iron. This disagreement between DFT calculated and expected values for J_{mag} has already been commented in the literature [28]. Anticipating on the "Results" section below, it is worth mentioning here that using DFT-calculated J_{mag} leads for Fe-Al to magnon corrections to configuration free energies 20 times lower than phonon corrections. This justifies including only the phonon contributions in non-configurational free energies.

II-4 Statistical thermodynamics approaches

Having established cluster Hamiltonians to describe the energetics of bcc-based Fe-Al-Mn-C, their thermodynamic validity was investigated by means of statistical methods.

In particular, the accuracy of the results depends on the choice made to evaluate the configurational entropy. To investigate this important issue, we resorted to various mean-field approximations (PMF [33], irregular tetrahedron CVM [46]) and compared them, as often as possible, to reference results provided by exact MC simulations. In addition, it is worth mentioning that a less standard and somewhat more elaborate PMF approach at constant C content was developed in this work, in order to study quaternary Fe-Al-Mn-C with atoms occupying both substitutional and interstitial lattices. For this kind of system, there is no natural way to include interstitial sites into the standard irregular tetrahedron CVM, and therefore this extension was carried out only within the PMF framework.

III Results

III-1 Binary Fe-Al

III-1.1 Optimization of configuration models

Following the methodology described previously, the first step consists in building an ab initio-based cluster model for bcc-based Fe-Al. The most "natural" model to consider, noted BCC-FeAl-SS2c0, is a "one-to-one" model in so far as the numbers of ASDB elements and required energy coefficients are equal. BCC-FeAl-SS2c0 attempts to describe the Fe-Al binary system using first- and second-neighbor pair interactions, the four coefficients J_{ϕ}, J_1^{Al} , $J_2^{1,AlAl}$ and $J_2^{2,AlAl}$ (subscript and superscript refer to cluster type, either point or pair, and interaction range) being determined from the ab initio energies of four supercells containing pure bcc iron, a single Al substitutional atom, and Al pairs either in first- or second-neighbor shells. A second model, labelled BCC-FeAl-SS2c1, is also characterized by the same four energy coefficients mentioned above, the values of which are however obtained adding ordered compounds (B2-FeAl, B32-FeAl and $D0_3$-Fe_3Al) as complementary structures into the ASDB. The values of the energy coefficients for both models are reported in Table 1. While the interaction energies of BCC-FeAl-SS2c0 directly correspond to the binding energies of Al pairs, the coefficients for the overdetermined BCC-FeAl-SS2c1 model are different from these binding energies. As mentioned above, these coefficients are therefore referred to as effective coefficients.

	BCC-FeAl-SS2c0	BCC-FeAl-SS2c1	BCC-FeAl-SS3c1	BCC-FeAl-SS4c1	BCC-FeAl-SS5c1
J_ϕ	-16.6105	-16.6100	-16.6104	-16.6104	-16.6104
J_1^{Al}	3.7933	3.7602	3.7837	3.7818	3.7781
$J_2^{1,AlAl}$	0.0882	0.1963	0.1961	0.1312	0.1348
$J_2^{2,AlAl}$	0.1131	0.0463	0.0462	0.0462	0.1079
$J_2^{3,AlAl}$	-	-	-0.0038	-0.0035	-0.0029
$J_2^{4,AlAl}$	-	-	-	0.0217	0.0205
$J_2^{5,AlAl}$	-	-	-	-	-0.0463

Table 1: Ab initio-based pair energy coefficients (eV) of the various cluster models considered in this work for bcc Fe-Al, including the effect of the ASDB (first two columns) and the pair interaction range.

A first glance on the respective merits of these models is conveniently obtained from their ground-state properties. To this aim, for second-neighbor pair models such as those presented here, it is common to display the stable 0 K structure map as a function of the first- and second-neighbor pair coefficients [33]. Plotting these coefficients on this ground-state diagram (Figure 1) shows that BCC-FeAl-SS2c0 predicts as a ground state the B32 compound instead of B2 observed experimentally. Conversely BCC-FeAl-SS2c1 is in reasonable agreement with the experimental phase diagram at moderate temperature. It is however important to keep in mind that comparison with experiments can only be done if temperature effects are taken into account. As mentioned previously, PMF offers a convenient way to easily estimate the validity of an energy model with respect to temperature, at least as concerns relative phase stabilities. Although the solubility limit is significantly underestimated and no two-phase domain is found, PMF confirms that the BCC-FeAl-SS2c1 model indeed provides reasonable agreement with the experimental phases for Fe-Al (Figure S3 in Supplemental Material).

While the content of the ASDB is therefore clearly a key-parameter to obtain models with good predictive capability, a second aspect requiring special attention concerns the

choice of the relevant clusters included in the Hamiltonian. Having chosen to restrict ourselves to pair interactions, and following the abundant literature on this topic [47-51], we focus on the effect of extending the range of these interactions up to fifth neighbors. The energy coefficients of the corresponding models are listed in Table 1. (Note that due to the presence of the complementary structures in the ASDB, all pair coefficients for these models differ from the binding energies displayed in the first column of Table 1.) Considering as previously the PMF phase diagrams (Figure S4 in Supplemental Material) reveals no significant difference between the various models.

On the whole, we are led to the couple of conclusions that (i) relevant ordered compounds are required in the ASDB, and (ii) interactions between substitutional elements can reasonably be restricted to second neighbours, which suggests that the BCC-FeAl-SS2c1 model is optimal for our purpose. To confirm this point, it should be recalled that, while PMF gives reasonable qualitative trends, more quantitative results can be obtained using the CVM and MC approaches. The latter approaches appear to be in remarkable agreement, both predicting solubility limits close to experiments and reproduce the A2-$D0_3$ two-phase domain (see Figure S5 in Supplemental Material). Conversely, the maximum $D0_3$ → B2 transition temperature consistently lies around 600 K in CVM and MC, namely an underestimated prediction with respect to experiments, which demonstrates that the good PMF prediction of the $D0_3$ → B2 transition temperature was fortuitous. Having thus identified for Fe-Al an energy model with good qualitative / semi-quantitative capabilities, we are thus in good position for our main task of increasing the chemical complexity towards Fe-Al-Mn-C. However, before pursuing in this direction, it is of particular relevance to conclude this study of Fe-Al by examining the influence of non-configurational temperature effects, in order to investigate their ability to provide a quantitatively more realistic description of the Fe-Al phase diagram.

III-1.2 Non-configurational temperature effects

Phonon contributions

As seen previously, ab initio-based first- and second-neighbor pair interactions are able to describe with a reasonable accuracy the bcc-based Fe-rich side of the Fe-Al phase diagram. However, these models underestimate the $D0_3$ → B2 transition temperature. In

order to determine if this effect is due to intrinsic deficiencies of the approach or to the lack of description of non-configurational effects, it is useful to investigate the influence of phonons and magnons on the predicted phase diagram. Adding these non-configurational free energy contributions to ASDB energies leads to temperature-dependent effective energy coefficients *J(T)*.

As for phonons, the spectrum calculated by DFT yields the vibration contribution to the free energy F_{vib} for each configuration included in the ASDB. Figure 2a, which presents these contributions obtained according to equation (2) in the framework of the harmonic approximation, shows that structures having similar compositions have similar F_{vib} contributions. Following this idea, we propose to attribute to the B32 compound the same vibration free energy as that calculated for B2, our harmonic analyses having revealed that B32 may be dynamically unstable (presence of imaginary vibration modes). Taking into account these assumptions, the temperature-dependent energy coefficients *J(T)* are displayed on Figures 3a and 3b, the corresponding model being labelled BCC-FeAl-SS2c1T. It should be noted that the four energy coefficients have monotonous temperature dependence, with an increasing (resp. decreasing) profile for pairs (resp. point and empty cluster).

The CVM phase diagram obtained using this approach is displayed on Figure 4a. Firstly, it is important to note that including phonons allows to preserve the phase diagram topology (same nature of domains and phases), which in itself constitutes a non-trivial result. Similarly, the A2 → B2 phase limit is also weakly modified. Conversely, a major change concerns the $D0_3$ → B2 transition temperature, which becomes overestimated with respect to the experimental value (1160 K instead of 820 K). When drawing such conclusions, it is important to keep in mind that in this work, the effect of phonons was only partially accounted for, since anharmonic effects and hence lattice expansion were overlooked. Taking these factors fully into account should probably induce enhanced mixing trends, thus promoting the A2 solid solution with respect to ordered phases.

On the whole, these trends suggest that including vibrational degrees of freedom gives a physical guide to produce more predictive phenomenological models by controlling (attenuating in the present case) phonon effects, as illustrated on Figure 4b, which displays the CVM phase diagram for a BCC-FeAl-SS2c1T390 model built by freezing

phonon contributions to their 390 K value (temperature-independent coefficients). This model is characterized by a $D0_3$ → B2 transition temperature remarkably close to the experimental one.

Magnon contributions

A comprehensive description including magnetic degrees of freedom and their interactions with phonons drastically raises the complexity of configurational energetics. Up to now, attempts towards this highly challenging issue have been carried out only for pure iron (fcc vs bcc competition) or binary alloys at a given composition. Having in mind to provide predictive models for chemically more complex systems (quaternary alloys with a significant composition range), we adopt here a more simple spin-wave description of spin fluctuations around the ferromagnetic ground-state of ASDB configurations. Within this description, the key-parameter is the exchange integral J_{mag} between nearest-neighbor spins, calculated here by DFT by comparing the energies of magnetic and non-magnetic configurations for each ASDB structure. Using these values and following the magnon approach [27] yields the ASDB magnetic free energies, which can then be included in the model in exactly the same way as phonons, thus bringing a magnetic correction to the temperature-dependent effective energy coefficients *J(T)*. The results for these magnetic corrections are represented on Figure 2b, which clearly shows that magnetic free energies are negligibly small compared to vibration contributions, and thus must have no influence on the predicted Fe-Al phase diagram.

III-2 Ternary Fe-Al-Mn

The previous results have demonstrated the good ability of short-range pair interactions, determined from ab initio calculations, to capture the main features of the thermodynamics of Fe-Al alloys with bcc structure. Following our route towards Fe-Al-Mn-C alloys more representative of currently used steels, the next step is now to include manganese, as a supplementary substitutional element competing with aluminium. The task of providing a reliable energy model for Fe-Al-Mn is made more difficult by the lack of experimental results on this system, especially phase stability, which strongly contrasts with the wealth of data available for bcc Fe-Al. As second-neighbour interactions between substitutional sites were found to be sufficient for Fe-Al, the same

interaction range is retained in presence of Mn. As before, the validity of this assumption will be checked through its consequences on the thermodynamic properties of Fe-Al-Mn. Care will also be taken to ensure that the ternary model constitutes a "natural" extension of the previous binary one, in particular by preserving a good predictive ability for Fe-Al.

III-2.1 Choice of ASDB

As already pointed out for Fe-Al, it remains essential to ensure the correctness of the choice of the ASDB in presence of Mn. Following our methodology, the initial ASDB for Fe-Al-Mn is thus built by providing the ab initio input data required exactly for the determination of the clusters involved in the model, namely the Mn point, the Al-Mn and the Mn-Mn pairs. This procedure guarantees that the binary Fe-Al part of the model is left unchanged when switching to the ternary system. Here again, this raises the issue of choosing the right magnetic state for these input data involving Mn. To this aim, assuming that the surrounding Fe atoms keep ferromagnetic order (magnetic moments close to 2.2 μ_B), we performed a detailed analysis of the influence of the initial Mn magnetic moments on the final energy and magnetic state for an isolated Mn atom in bcc Fe. This analysis shows that a final antiferromagnetic state is reached for Mn (μ_{Mn} = -2 μ_B) while the magnetic moments of surrounding Fe remain almost unaltered. This final state is reached from different initial μ_{Mn} including μ_{Mn} = 0, and the latter initial value was therefore adopted as a starting point for all alloy configurations involving Mn.

The pair energy model built from these ab initio magnetically optimized data is labelled BCC-FeAlMn-SS2c1, and its validity must be tested against the few experimental data available, namely the aforementioned $L2_1$ → B2 → A2 order-disorder sequence occurring at Fe_2AlMn composition. To check this point, we employ canonical (NVT) MC simulations (12x12x12 bcc supercell) at this composition, and monitor the occupancies of the four usual bcc sublattices (displayed on Figure 1b) as function of temperature. These results (not shown for brevity) point out erroneous phase stability, with the low-temperature emergence of an XA ordered compound not observed experimentally. It should be noted that the competition between $L2_1$ and XA orderings in Heusler alloys is a well-documented fact. This disagreement confirms the necessity,

already noted for binary Fe-Al, to feed the energy models with complementary ordered structures, which is fully consistent with the procedure generally employed to build cluster expansions. Adding the $L2_1$ and XA compounds, together with pure bcc Mn, to the ASDB results in a new energy model labelled BCC-FeAlMn-SS2c2. With this model, the MC study of thermal phase stability at Fe_2AlMn composition (Figure 5) shows that the right disordering sequence is now obtained. The predicted transition temperatures (1100 K for $L2_1$ → B2 and 1500 K for B2 → A2) are in reasonable agreement with their experimental counterparts, respectively 898 K and 1577 K determined from calorimetry measurements [4]. It is also noticeable that the B2 → A2 temperature predicted from BCC-FeAlMn-SS2c2 takes a much more reasonable value than previously obtained (4000 K) for BCC-FeAlMn-SS2c1. On the whole, the BCC-FeAlMn-SS2c2 ternary model appears to be quite satisfactory, which confirms that second-neighbour interactions are indeed sufficient for substitutional Fe-Al-Mn. Finally, it is instructive to compare the energy coefficients for the two previous ternary models. As shown in Table 2, adding the $L2_1$, XA and bcc Mn complementary structures to the ASDB has a negligible influence on the binary Fe-Al part of the energetics, which offers a satisfactory picture for the proposed modelling, in the same line as used in more phenomenological (Calphad-type) approaches, for which higher-order systems are built from lower-order ones. Conversely, the ternary model itself, as expected, is very sensitive to the energies of ASDB structures containing Mn atoms.

	BCC-FeAlMn-SS2c1	BCC-FeAlMn-SS2c2
J_ϕ	-16.6100	-16.6102
J_1^{Al}	3.7602	3.7605
J_1^{Mn}	-0.5691	-0.4926
$J_2^{1,AlAl}$	0.1963	0.1962
$J_2^{1,AlMn}$	-0.0289	0.0161
$J_2^{1,MnMn}$	0.1441	-0.0174
$J_2^{2,AlAl}$	0.0463	0.0462

$J_2^{2,AlMn}$	0.1445	-0.0284
$J_2^{2,MnMn}$	0.1536	-0.0032

Table 2: DFT-based pair interactions (eV) for bcc Fe-Al-Mn, for two different ASDBs noted c1 and c2.

To complete our investigations of the ternary BCC-FeAlMn-SS2c2 model, the 973 K (a temperature chosen due to its practical interest) isothermal section of the ternary phase diagram is built by means of PMF and CVM calculations, and the results are displayed on Figure 6. Comparing both approaches shows that the PMF predictions (Figure 6a), although quantitatively insufficient, roughly respect the presence of the various phases, except the B32 domain on the Al-Mn line, which is peripheral for our work. The Fe-Al line of the ternary phase diagram totally agrees with the binary one (Figures S3b and S5a in Supplemental Material). Finally, the accuracy of these thermodynamic calculations is checked by means of exact grand canonical MC simulations. Due to the computational time required for such simulations, an exhaustive MC plot of the phase diagram is not possible, and we thus focus on a single isopotential line performed by varying the Al effective chemical potential μ_{Al} at constant μ_{Mn}. Figure 6b, which shows this isopotential superposed to the CVM phase diagram, clearly demonstrates the accuracy of the latter approach to investigate the thermodynamic properties of this ternary system.

III-2.2 Influence of phonons

		T($L2_1$ → B2)	T(B2 → A2)
BCC-FeAlMn-SS2c2	PMF	1350	2600
	CVM	1100	1600
	MC	1100	1500
BCC-FeAlMn-SS2c2T	PMF	1000	1200
	CVM	850	2500
	MC	850	2550
Experimental [4]		898	1677

Table 3: Order-disorder transition temperatures (K) at composition Fe_2AlMn, as predicted by the various present models and compared with earlier experimental measurements.

As for binary Fe-Al, the influence of atomic vibrations on the ternary energy coefficients (i.e. those involving Mn) was investigated using the harmonic approximation (Figures 3c and 3d, and insert of Figure 3a). Contrary to Al ones which remain unchanged with respect to those determined for the binary model, the temperature variation of those coefficients associated to Mn displays some dispersion due to numerical noise, which however is not critical for our purpose. Interestingly, for Mn as well as Al, the effect of temperature on pair coefficients (increase) is opposite to that obtained for point and empty clusters (decrease). As previously for Fe-Al, phonons in ternary Fe-Al-Mn have a non-negligible effect, which gives rise to a new temperature-dependent BCC-FeAlMn-SS2c2T energy model tested against phase stability at Fe_2AlMn composition by PMF, CVM and canonical MC simulations (not shown for brevity). The results for the transition temperatures are gathered in Table 3, which indicates that the T-dependent model allows for a better description of the $L2_1$ → B2 transition, whereas it clearly overestimates the B2 → A2 order-disorder temperature. This contrasts with binary Fe-Al presented previously: in the latter case, phonons were found to have a strong influence on ordering, the $D0_3$ → B2 transition temperature lying respectively around 600 K and 1150 K for the BCC-FeAl-SS2c1 and BCC-FeAl-SS2c1T models (experimental value ~ 800 K), whereas they led to only slight modifications of the B2 → A2 transition temperature, around 1600-1700 K for both models at Fe_3Al composition (experimental value ~ 1200 K), by extrapolating at higher T the data of Figures S5a and 4a. This strikingly detrimental role of phonons on the modelling of the B2 → A2 transition in the ternary alloy suggests that phonons may not be well taken into account in the A2 solid solution including Mn, possibly in reason of strong anharmonicities induced by this element (neglected in the present harmonic approach). Alternatively, this disagreement may also be interpreted as an effect, overlooked in the present approach, of Mn-induced magnon-phonon interactions. Further studies devoted to the coupling between phonons and magnetic partial disorder may be useful in elucidating these intricate issues, and should thus help reach more realistic thermodynamic description of Al- and Mn-doped steels. On the whole, whereas

this panel of intricate trends on phonon and magnon effects in Fe-Al and Fe-Al-Mn clearly illustrates that a long way still has to be gone until non-configurational degrees of freedom are reliably handled in alloy energetics, these effects do not appear to critically question the overall phase stability deduced from the present modelling, which is a non-trivial result a priori. As a consequence, the BCC-FeAlMn-SS2c2 model can reasonably be regarded as sufficiently realistic to provide a sound basis for tacking the addition of carbon, the topic of the next section.

III-3 Quaternary Fe-Al-Mn-C and influence of C-C interactions

Having achieved a reliable model for ternary bcc Fe-Al-Mn, the following step consists in taking into account carbon, in order to reach a thermodynamic modeling of Al- and Mn-doped steels with bcc ferritic structure. For several reasons, the introduction of C however significantly raises the level of difficulty of such modeling. Firstly, as concerns the required ab initio input data, the interplay between supercell size and range of pair interactions is probably more critical in presence of C, since such interstitial elements are expected, more than substitutional ones, to induce severe elastic long-range strain fields, possibly difficult to capture in ab initio methods using periodic systems with limited size. Secondly, the lack of experimental data, already pointed out for ternary Fe-Al-Mn, becomes even more drastic in quaternary Fe-Al-Mn-C, as for (i) the role of C and C-C interactions in bcc iron, (ii) the interactions between C and substitutional elements. This strikingly contrasts with the abundant literature devoted to studying the fcc-based κ-Fe_3AlC "kappa" phase in austenite, including subtle features such as C off-stoichiometry, Fe-Mn competition in presence of Mn, or the stabilizing effect of its coherent interfaces with the matrix [52]. In this context, it becomes highly non-trivial to achieve realistic thermodynamic models for the ferritic steels considered here. To maintain a sufficient degree of internal consistency in the present work, we thus decide to go further in our choice of limiting as much as possible the range of pair interactions. For clarity reasons, the study of the role of C will be performed in two steps, namely (i) by considering solely "S-I" interactions between substitutional elements and interstitial C, and (ii) by including "I-I" interactions between interstitial atoms.

In presence of carbon, obtaining reliable ab initio input data for the ASDB may become more intricate. Firstly, it is clear from Figure 7 that, even for an isolated C atom in bcc

iron, the grand canonical insertion energy for this interstitial species does not converge with supercell size as easily as for substitutional ones. To maintain tractability with the available computational resources, we however decide to keep for ab initio supercells with carbon the same 4x4x4 size as used previously for binary and ternary alloys. Moreover, as detailed below, while the ab initio calculations of Al-C and Mn-C pair energies suggest that the second-neighbour range can be adopted for S-I interactions (in agreement with the previous S-S part of our modeling), this hypothesis will be more questionable for I-I interactions between C atoms, probably in reason of the larger elastic field associated with interstitial species. In a first step, we however limit C-C interactions to the second-neighbour range. This leads to build two distinct models for quaternary Fe-Al-Mn-C, respectively labelled BCC-FeAlMnC-SS2SI2c2 and BCC-FeAlMnC-SS2SI2II2c2. In a second step, we will then examine the validity of this assumption about C-C interactions, by adding the S-centered 4^{th}-neighbor C pair (i.e. centered by a substitutional site), a choice justified by previous theoretical studies [7].

	BCC-FeAlMnC-SS2SI2c2	BCC-FeAlMnC-SS2SI2II2c2

J_{ϕ}	-16.6102	-16.6102
J_{1S}^{Al}	3.7605	3.7605
J_{1S}^{Mn}	-0.4926	-0.4926
J_{1I}^{C}	-8.5162	-8.5162
$J_{2SS}^{1,AlAl}$	0.1962	0.1962
$J_{2SS}^{1,AlMn}$	0.0161	0.0161
$J_{2SS}^{1,MnMn}$	-0.0174	-0.0174
$J_{2SS}^{2,AlAl}$	0.0462	0.0462
$J_{2SS}^{2,AlMn}$	-0.0284	-0.0284
$J_{2SS}^{2,MnMn}$	-0.0032	-0.0032
$J_{2SI}^{1,AlC}$	0.6575	0.6575
$J_{2SI}^{1,MnC}$	-0.0903	-0.0903
$J_{2SI}^{2,AlC}$	0.3652	0.3652
$J_{2SI}^{2,MnC}$	0.0145	0.0145
$J_{2II}^{1,CC}$	-	1.8852
$J_{2II}^{2,CC}$	-	0.7659

Table 4: Pair interactions (eV) for bcc Fe-Al-Mn-C, either neglecting (left column) or including (right column) C-C interactions between interstitial carbon atoms, as deduced from ab initio calculations and pair models.

In this framework, before investigating more generally the C behaviour in quaternary Fe-Al-Mn-C, it is an instructive preliminary task to explore the ground-state 0 K properties of bcc Fe-C, using the aforementioned set of pair interactions. It is noteworthy that such theoretical information about C in ferrite, to our knowledge, has never been provided hitherto, in spite of its basic and informative character. Indeed, the contrast is striking with its austenite counterpart (C in fcc Fe) for which theoretical

studies have been performed, leading to useful results on carbides in fcc transition metals [53]. This difference of treatment can be attributed to two reasons, (i) the low C solubility in ferrite before the emergence of other competing phases, and (ii) the somewhat more complex crystallography involved in the bcc case. More precisely, since fcc-based compounds containing C (and more generally interstitial elements) have a NaCl structure consisting of two interpenetrating fcc lattices, the same fcc ground-state analysis, already described in the literature [54], applies to both S and I elements, which greatly simplifies the problem. Conversely, in the bcc case the I sites (a set of six I octahedral sites in the two-site bcc cubic cell, as displayed on Figure 1) do not have a bcc structure, hence requiring for I sites a specific analysis absent from the previous studies. In our work, we do not attempt to provide the formal developments for such an analysis, but instead we restrict to explore numerically the ground-state properties of bcc Fe-C using first- and second-nearest neighbor C-C interactions. The determination of ground states for bcc Fe-C is carried out by exhaustive scan of the energetics among the $2^6 = 64$ configurations possible for C in a single bcc unit cell with six I sites, hence a maximum carbon content x_C equal to 0.75 (formula Fe_2C_6). Figure 8 displays the results of this ground-state analysis, namely the C content and the filled I sites as a function of the C chemical potential. To be more informative, we perform this analysis (i) using only the first-neighbour C-C interaction, and (ii) by including also the second-neighbour one. In the first case (Figure 8a), the only intermediate composition allowed is x_C=0.6 (Fe_2C_3), with two equivalent variants obtained by filling either the interstitial sublattices (I1,I2,I3) or (I4,I5,I6). Including the second-neighbour interaction (Figure 8b) allows a second intermediate composition x_C=0.5 to emerge, with three equivalent variants, since crystal symmetry (see Figure 1) implies the equivalence of filling with C either of the (I1,I5), (I2,I6) and (I3,I4) pairs of sublattices. This simple picture should be kept in mind when performing more elaborate investigations (see below). Remarkably, the second-neighbour interaction provides a filling of I sites by pairs, contrary to the "triplet" filling due to first-neighbour C-C interactions.

When going to thermodynamic modelling, the CVM approach cannot be used in presence of interstitial carbon, since no CVM formalism including octahedral interstitial and substitutional sites is currently available. We therefore resort to the PMF approximation, since the latter has demonstrated for Fe-Al and Fe-Al-Mn its ability to

reveal reasonable semi-quantitative trends on phase stability and competition. As shown below, the validity of our PMF calculations will however be controlled by means of exact MC simulations. In order to keep as close as possible to more phenomenological thermodynamic modellings of steels, in which isothermal sections of phase diagrams are performed at constant C content, we make use of a mixed canonical/grand canonical PMF formalism developed for this purpose, allowing to control the atomic fraction of carbon, while the other elements Al and Mn remain, as previously, controlled through their chemical potentials.

The energy coefficients of the two quaternary models are displayed on Table 4. As a consequence of the absence of ordered compound involving C in the ASDB, the "ternary" coefficients of each model are not affected by the presence of C (compare with Table 3). While Al-C interactions moderately decrease while remaining repulsive both for first- and second-neighbour shells, the first-neighbour Mn-C interaction is attractive and decays strongly when reaching the second-neighbour shell. Noticeably, this behaviour justifies the aforementioned hypothesis of limiting Al-C and Mn-C interactions to second-neighbour range. Moreover, in agreement with earlier theoretical results [7], the interactions between C atoms are expected to be strongly repulsive. Their effect is investigated through their consequences on thermodynamic properties, especially their influence on the stability of the previously mentioned bcc-based phases (via isothermal sections of quaternary phase diagrams), and on carbon site occupancies.

In absence of I-I interactions (model BCC-FeAlMnC-SS2SI2c2), the form of the PMF equations implies (and it will be confirmed by the exact MC simulations, see below) that only two kinds of I sublattices have to be distinguished. More precisely, the I1, I2 and I3 sublattices necessarily have identical C occupancies, and a similar remark holds for I4, I5 and I6. The study can therefore be restricted to I1 and I4. Whereas experimentally, due to competing phases such as austenite and cementite, the solubility limit of C in ferrite is low, it is instructive to keep a larger window of exploration for the C content, thus allowed to reach ~10 at.%. Keeping the same temperature as previously (973 K), isothermal sections at fixed C content can easily be obtained from PMF calculations, and the results for 5 at.% C are displayed on Figure 9. It is striking to remark that the presence of C (5 at.%) does not modify significantly the stability of the phases previously detected in ternary Fe-Al-Mn (compare Figure 9 and Figure 6a).

Conversely, the C occupancies on the I sublattices are (I1=I2=I3)≠(I4=I5=I6), showing that C in Al- and Mn-doped ferrite is characterized by long-range order throughout the whole composition domain (Figure 9b), which reflects the strongly different Al-C and Mn-C interactions. It is worth noting that C ordering is also present on the binary limits of the phase diagram, in particular the Fe-Al one of high practical importance. More precisely, while our PMF calculations at 973 K (insert of Figure 9b) indicate that C in pure bcc Fe should form a solid solution (identical occupancies for all I sites), they also reveal that a critical Al content ~5 at.% entails C ordering. Comparing Figure 9a and the insert of Figure 9b shows that this critical Al content also corresponds to the A2 → B2 transition, hence there is a correlation between the orderings for substitutional atoms and for interstitial C. Due to the lack of information on such coupling effects from phenomenological (Calphad-type) approaches [17], experimental investigations of Fe-Al-C would be useful to check these features and the accuracy of the present modelling.

Because of the limited predictive power of the PMF approach, the validity of these results must be checked by means of exact MC simulations at 973 K and composition $FeAlC_x$, using a 6x6x6 supercell containing 432 substitutional sites and 1296 interstitial sites (6 million steps for equilibration, 12 million steps for thermal averages). The Al and C site occupancies are monitored as a function of the C content between 0 and 12 at.%. In agreement with the PMF phase diagram of Figure 9a drawn for 5 at.% C, the B2 compound remains stabilized throughout the entire composition range explored (Figure 10a, top). Moreover, although the MC results on C occupancies (Figure 10a, bottom) show a non-negligible dispersion (due to difficult MC sampling), they are in good agreement with the PMF trends pointing out two groups of three equivalent I sublattices. Finally, it is worth noting that increasing the amount of C entails a lowering of the long-range B2 order on S sites. On the whole, these consistent PMF vs MC trends for the BCC-FeAlMnC-SS2SI2c2 give good confidence when extending the PMF analysis in presence of C-C interactions.

The effect of including the interactions between interstitial C, which corresponds to the BCC-FeAlMnC-SS2SI2II2c2 model, is thus investigated along the same lines as previously, namely by determining by PMF the isothermal phase diagrams at constant C atomic fraction. The negligible effect of C on S-site ordered compounds is confirmed (not shown since very similar to Figure 10a), a satisfactory feature since the S-I part of

the model is not changed when including I-I coefficients (see Table 4). Conversely, the behaviour of C is substantially modified by the presence of I-I interactions (Figure 11a), only two sublattices (I1 and I5) being then occupied. Other features previously noted for S-I interactions alone are however unchanged, in particular the C ordering through the major part of the composition domain at 973 K, and the Al critical level required for C ordering in Fe-Al-C (insert of Figure 11a). PMF calculations also offer a convenient way to compare the order-disorder behaviours on S and I sites as a function of temperature. Figure 12 thus displays the loss of C ordering across the transition temperature (for 5 at.% C), the latter being found between 1400 and 1450 K for PMF. The two main kinds of C orderings already mentioned are also depicted, namely "2-interstitial-sublattice" (2Isl) ordering, i.e. preferential occupancy of I1 and I5 sublattices (or other equivalent variants (I3,I4) and (I2,I6) of the same C ordering), and "3-interstitial-sublattice" (3Isl) ordering, i.e. I1=I2=I3 and I4=I5=I6.

Using the same conditions as previously for BCC-FeAlMnC-SS2SI2c2, the validity of these PMF predictions including I-I interactions is then investigated via MC simulations providing the C occupancies in the various I sublattices of $FeAlC_x$ (Figure 10b). It confirms that S occupancies, as expected, remain unaltered by I-I interactions. Moreover, the presence of a pair (I1 and I5) of occupied sublattices is also noticed. This demonstrates that this feature is really induced by I-I interactions, thus not being a PMF artifact, which emphasizes the relevance of the latter approach. On the whole, PMF thermodynamics, in spite of its simplicity, offers a convenient way to investigate bcc Fe-Al-Mn-C.

To conclude this analysis of the second-neighbour quaternary model for Fe-Al-Mn-C, it is useful to explore the respective effects of S-I and I-I interactions on C ordering in Al- and Mn-doped ferrite. To this aim, Al-C and/or Mn-C interactions were selectively switched off, leading to the results summarized on Figure 11. Firstly, cancelling all S-I interactions (Figure 11b) consistently leads to C atoms insensitive to the content of substitutional species, hence constant I1 and I5 occupancy levels. Conversely, selectively switching off Mn-C interactions (Figure 11c) leads to an S-induced modulation of C occupancy close to that obtained for the full quaternary model (Figure 11a), which can be easily understood from the moderate value of Mn-C interactions (Table 4). Finally, retaining only Mn-C interactions proves to have a much more

significant effect on C (Figure 11d), with a complete change of the modulation profile, however keeping only the I1 and I5 sublattices occupied, in agreement with the above ground-state properties (Figure 8b) for the chosen C content (figured out by the dashed line on Figure 8).

As recalled on Figure 13a, previous ab initio calculations [7] of the binding energy of the C-C pair with various neighbourhoods have pointed out that the role of the 4S interaction (4^{th}-neighbor pair centered with an S site) might be unexpectedly large. It seems therefore logical to explore the influence of 4S interactions on the results deduced from the 2^{nd}-neighbour models presented above. Firstly, the influence of the 4S interaction on the 0 K ground-state properties of bcc Fe-C is thus investigated similarly to Figure 8 (using +0.8 eV and +1.7 eV as test-values suggested by earlier work [7]), showing that the 4S effect with respect to the SS2SI2II2 model (Figure 8b) is rather small, limited to a chemical potential offset without change of the type of C occupancies. Turning to PMF calculations, the effect of gradually switching on the 4S interaction on the C behaviour at 973 K is displayed on Figure 13b. A threshold is found for *J(4S)* ~1 eV, with strong enhancement of C occupancies on two supplementary sublattices (I2 and I3 for the I1-I5 variant shown on Figure 13). This leads to the emergence, clearly visible along the Fe-Al axis, of a domain with I1=I2=I3 and I4=I5=I6, namely a behaviour already detected in absence of I-I interactions (Figure 9b). This domain gradually extends up to the whole composition range for *J(4S)* ~1.3 eV. For values > 1.3 eV (consistent with the results of [7]), the behaviour is not significantly affected by further increase of *J(4S)*. On the whole, while our results suggest that C-C interactions beyond second neighbor may play a role in the behaviour of C in ferrite, the large 4S value previously proposed [7] should deserve further confirmation, due to the presence of long-range elastic effects possibly interfering with the limited supercell used in the ab initio calculations.

IV Discussion

The objective of this work was to produce an energy model at the atomic scale able to predictively describe the thermodynamics of “realistic” systems as complex as ferritic steels containing four chemical elements placed in two types of atomic sites, substitutional and interstitial ones. The method most widely employed to study such

complex systems is probably the Calphad method, which presupposes for the free energy a functional form which is then adjusted to available experimental or computational data. In this work we chose an approach based on the construction of a Hamiltonian that directly describes the chemical interactions between atoms, and from which measurable quantities (phase diagrams, short- and long-range order,…) can be determined. In its current form, the model allowed us to study the ordering of carbon in a quaternary Fe-Al-Mn-C ferritic alloy. Beyond this point, the success in building this tool makes it possible to envisage an extension of the methodology to determine kinetic properties such as atomic migration energies in similarly complex systems.

Building a Hamiltonian able to accurately and predictively describe a quaternary system at the atomic scale appears to be a delicate task requiring a sufficient control of the different approximations that must necessarily be introduced. A first main choice of this work was to use DFT energy calculations to determine the energy coefficients of the model. In itself, using DFT involves various approximations inherent to this method, the far-reaching consequences of which are difficult to measure. Only the intensive use of these methods since their development has allowed establishing their real predictive character in the field of metallic alloys. However, sources of inaccuracy remain on the choice of the exchange-correlation functional and practically tractable computational conditions (size of supercells, bases for development of Kohn-Sham orbitals, discretization of reciprocal space). A second level of approximation in the present work concerns the choice of the type of Hamiltonian (pairs, triplets ...) to describe configurational (free) energies, which remains delicate and requires a confrontation with experimental data to determine its predictive character. In this context, faced with a rather large chemical complexity, we chose to restrict our study to pair Hamiltonians, which proved sufficient to produce reasonably predictive models for bcc Fe-Al-Mn-C alloys.

The study of the Fe-Al binary system first allowed us to verify that combining DFT calculations with pair Hamiltonians to build phase diagrams was successful. In this system, for which there is an abundant literature, we showed that sufficiently predictive models can be obtained by limiting the range of interactions to second neighbors. Taking into account non-configurational effects through the harmonic approximation for phonons has a significant effect on the phase diagrams and shows a way to produce

"phenomenological Hamiltonians" which describe more quantitatively experimental data.

The same framework for energy model construction also proved its efficiency in the more complex case of ternary Fe-Al-Mn alloys, by preserving the gains of the binary model and showing a good predictive character with regard to the little available experimental information.

As a further step towards more realistic ferritic steels, the development, along the same methodology, of quaternary models including carbon in interstitial position, allowed us to study in a wide range of chemical composition the correlation between the ordering of substitutional atoms and that of interstitial carbon, taking into account the strongly repulsive interactions between neighbouring carbon atoms.

In particular, our model predicts a fairly complex ordering of interstitial carbon at temperatures of practical interest, in interplay with the content of substitutional elements. These results obtained by PMF calculations were confirmed by exact MC simulations over a narrower compositional range. While no experimental data allow to measure their degree of validity, these predicted trends are at odds with current phenomenological modellings by the Calphad approach, since the latter generally consider a unique interstitial lattice for C.

While our second-neighbor pair modelling has proved to be robust for Al and Mn substitutional elements, its relevance could nevertheless be questioned in presence of interstitial C, because of the high repulsive fourth-neighbor C-C interactions highlighted by previous ab initio calculations [7]. Given the uncertainties of the fourth-neighbor interactions due to unavoidably limited supercell sizes, we performed a parametric study of the influence of this interaction, which showed that the ordering of interstitial C remains, although possibly changing of nature. Experimental measurements of C ordering would be a useful way of clarifying this important issue of fourth-neighbor C-C interaction in ferrite.

While this work is mainly concerned with chemically complex alloys, it should be noted that the intricacy level is raised further by the presence of magnetic interactions, clearly illustrated on the Fe-Al diagram (figure S1) by the presence of a ferromagnetic (FM) → paramagnetic (PM) transition line, which crosses the various domains of chemical

order. In particular, from figure S1, it appears that a large part of the Fe-Al equilibria investigated in this work lie in the paramagnetic domain. For our purpose, the consequences of neglecting PM phases might be more critical on the main solid- solid equilibria ($D0_3$-B2 and B2-A2, and to a lesser extent the A2 + $D0_3$ two-phase domain), since the energetic and magnetic models proposed in our work are based on DFT energetics using FM Fe for the ordered phases, while B2 is fully PM in its stability domain, and so is $D0_3$ except at low temperature. In this context, our choice of building our approach upon the ab initio energetics of FM A2, B2 and $D0_3$ phases lends itself to justification. Indeed, it is consistent with the general framework of configurational thermodynamics, in which non-configurational (magnetic, vibrational and electronic degrees of freedom) are neglected, at least in a first step. In this framework, it is logical to build the energy models (cluster Hamiltonians) from 0 K ab initio energetics, which in the present case implies to select FM A2-Fe, B2-FeAl and $D0_3$ Fe_3Al for this task. The opposite choice would obviously consist in introducing PM (free) energies into the ASDB. However, the procedure in this case would be then less well-defined and less easy to apply, requiring some extra modelling of the PM state for each element of the ASDB. Since we are interested in solid phase equilibria at moderate temperatures, it is a reasonable assumption that the FM vs PM free energy difference for the ordered compounds may not be too high at these temperatures. Although some checking of this hypothesis would be welcome, this is however beyond the scope of our work and does not question the global validity of our approach. Our choice ensures that the modelling is correct at low T and allows more or less phenomenological refinements for larger T, by adding T-dependent contributions such as phonons and magnons to lead T-dependent cluster models, as proposed in this work. Strictly speaking, restricting non-configurational factors to harmonic phonons and magnons is insufficient, but further refinements are challenging enough to offer much room for future investigations. Moreover as shown above for Fe-Al and below for Fe-Al-Mn, our work suggests that valuable information can also be obtained from such “first-order” corrections.

A cornerstone of our approach was the ab initio structure database, as regards both the relevant structures that it should include and the energies that should be affected to them. The latter point was found especially critical for isolated clusters (points, pairs) in otherwise pure bcc Fe, since these configurations correspond to a tricky interplay

between two effects, namely the convergence with respect to the ab initio supercell size, and the intuitive decay of pair energies with increasing neighbor range. Indeed, these two effects are really difficult to disentangle: even for reasonably large supercells such as those used above, the expected decay of binding energies with the pair distance could not always be evidenced without ambiguity, and performing elasticity corrections did not really clarify the situation. From this point of view, it is likely that the quality of the energy spectrum from the ab initio database could be refined, by resorting to much larger computational resources (thousands of atoms). This was however not the scope of the present study, since our primary goal was rather to proceed to an a posteriori check of the modelling through its merits for thermodynamic properties. Keeping this in mind, the selected methodology was successful.

Our study also pointed out the remarkable accuracy of the CVM approach for the modelling of Fe-Al and Fe-Al-Mn substitutional alloys. In view of this success, an appealing extension of our work would doubtlessly be to design a more general CVM scheme including the interstitial sites occupied by C. The difficulty of this task should however not be underestimated, since it would imply to take into account S-I as well as I-I interactions, hence the requirement to determine the relevant clusters including S and/or I sites, which probably constitutes a difficult crystallography issue. Moreover, the elegant formulation of the tetrahedron CVM approximation for substitutional alloys should no longer be valid in presence of interstitial sites, which may oblige to resort to a completely new formulation. In this context, the Point Mean-Field scheme proposed in the present work offers a convenient way to overcome these difficulties, while remaining a rather reliable guide for qualitative and semi-quantitative trends.

While our work was dedicated to bcc-based ferritic steels, the same methodology could obviously be applied to fcc-based austenitic alloys. Achieving this task would offer the tools required to investigate equilibria between bcc and fcc phases, hence providing information directly comparable to “realistic” equilibrium phase diagrams obtained either from experiments or from Calphad-type simulations. However, modelling fcc-based systems would imply to correctly handle the magnetic states of Fe in austenitic steels, which is by no means a trivial task. Previous studies have already demonstrated the intricacy of this issue in pure fcc iron: (i) considering only non-magnetic (NM), ferromagnetic (FM) and antiferromagnetic (AFM) states, ab initio calculations [55]

indicate that the most stable state is probably FM, (ii) when double-layer AFM ordering is taken into account, the latter becomes the new ground state [56], although this result is still matter of debate [57].

Our results about carbon behaviour in ferritic steels may usefully be compared with those of several earlier theoretical works on Fe-C, as described above in the introduction, predicting the existence of diluted Fe-C compounds stabilized by long-range elastic interactions. Our model, relying on shorter-range C-C interactions (up to fourth neighbours), is not designed to provide all the elements to discuss the stability of these diluted Fe-C compounds. However, predicting a strong energy increase above ~25 at.% C, it leads to an overall convex 0 K energy-composition curve for bcc Fe-C (see Figure S6 in Supplemental Material), and is thus qualitatively consistent with the previously pointed out trends of possible stability for such compounds, a similar agreement being obtained if 4S-type C-C interactions are switched on. It should however be noted that previous thermodynamic investigations of Fe-C were usually carried out using the "three sublattice" description, each sublattice itself consisting of two classes of sites (e.g. I1 and I5 in the above notation), whereas our work points out the possibility of distinct occupancies for each site of the pair, as illustrated above by mean-field and Monte-Carlo simulations. Such features, which appear to be entailed by the presence of substitutional elements (as suggested by Figure 11), may require further studies. Finally, while acquiring a more refined knowledge of the C-C interactions in Fe is indeed an interesting and challenging issue, our primary interest in the present work is somewhat different, being concerned with the effect of C in a ternary substitutional alloy, in order to investigate how interstitial C does interact with the substitutional elements, an issue scarcely investigated hitherto.

V Conclusion

In this work, we have demonstrated the good ability of ab initio-based pair models for building, from the atomic scale, a reasonable thermodynamic description of chemically complex alloys including substitutional and interstitial elements. To this aim, we have considered the specific case of Al- and Mn-doped ferritic steels of interest in automobile industries. As a main advantage, our approach allows to control the relevance of the various approximations added gradually (selection of ab initio database, range of pair

interactions, approximation for the entropy, phonon and magnon non-configurational degrees of freedom…). The modelling for bcc-based Fe-Al and Fe-Al-Mn substitutional alloys could be conveniently achieved by limiting pair interactions to second-neighbour range, which provided results in remarkably good agreement with experiments, for highly documented Fe-Al as well as for the more scarcely studied Fe-Al-Mn system. While the accuracy of the Cluster Variation Method (CVM) was checked by comparison with exact Monte-Carlo simulations, the much more tractable Point Mean Field (PMF) approximation was also used, and despite its limited predictive power for quantitative values, it proved to be a valuable guide, due to its good potential to provide quickly the main trends as regards phase stability. In absence of a CVM scheme for the more intricate case of Fe-Al-Mn-C ferritic steels, this type of quaternary system was thus investigated successfully with PMF, leading to a clear-cut description of C ordering and its coupling with the substitutional elements. These predictions should be useful in refining the widely used Calphad-type phenomenological models for these ferritic steels.

ACKNOWLEGDMENTS

This work was performed in the framework of the ANR-13-RMNP-0002 MeMnAl Steels funded by the Agence Nationale de la Recherche (ANR). This project was also supported by the competitive cluster “Materalia”.

FIGURE CAPTION

Figure 1: Predicted ground-state diagram of the various Fe-Al, Fe-Mn and Al-Mn systems considered. The insert displays the labelling of sublattices in bcc structure, including substitutional (four sublattices) and interstitial octahedral (six sublattices) sites.

Figure 2: (a) Ab initio harmonic vibration free energies and (b) magnon free energies of structures from the Fe-Al ASDB (using ab initio magnetic exchange parameters).

Figure 3: Temperature dependence of pair interactions for bcc Fe-Al-Mn: (a) empty cluster and Al point, (b) Al-Al pairs, (c) Al-Mn pairs, (d) Mn-Mn pairs. The insert of Figure (a) displays the behaviour of Mn point (for comparison, the Al point coefficient is also recalled).

Figure 4: CVM-predicted Fe-Al phase diagrams for models with temperature-dependent pair interactions: (a) BCC-FeAl-SS2c1T with fully T-dependent interactions, (b) BCC-FeAl-SS2c1T390 with interactions frozen at 390 K.

Figure 5: Predicted sublattice occupancies at Fe_2AlMn composition, using the BCC-FeAlMn-SS2c2 model and Monte-Carlo simulations.

Figure 6: Predicted 973 K isothermal sections of the bcc Fe-Al-Mn phase diagram, using the BCC-FeAlMn-SS2c2 model and (a) PMF, (b) CVM calculations. The isopotential on Figure (b) was obtained from Monte-Carlo simulations for purpose of checking the accuracy of our CVM results.

Figure 7: Grand canonical insertion energy of octahedral interstitial C in bcc Fe as a function of supercell size, from ab initio calculations.

Figure 8: Ground-state analysis (i.e. C content versus C chemical potential at 0 K) of bcc Fe-C using (a) first-neighbour C-C interactions only, (b) first- and second-neighbour C-C interactions. Also indicated are the C occupancies (0 or 1) of the six interstitial sublattices, including obvious degeneracies entailed by crystal symmetry (cf. Figure 1b).

Figure 9: Using the BCC-FeAlMnC-SS2SI2c2 model (no I-I interactions), PMF-predicted isothermal section (973 K) of Fe-Al-Mn-C with 5 at.% C: (a) S-site ordering, (b) I-site ordering. The insert of Figure b displays the behaviour on the Fe-Al axis.

Figure 10: Monte-Carlo simulations (T = 973 K) of sublattice occupancies in B2-$FeAlC_x$ using (a) the BCC-FeAlMnC-SS2SI2c2, (b) the BCC-FeAlMnC-SS2SI2II2c2 model (top: Al on S sites, bottom: C on I sites).

Figure 11: Influence of selective C-X (X=Al,Mn) interactions on C sublattice occupancies in Fe-Al-Mn with 5 at.% C: (a) fully interacting BCC-FeAlMnC-SS2SI2II2c2, (b) BCC-FeAlMnC-SS2SI0II2c2 with no C-X interactions, (c) BCC-FeAlMnC-SS2SI2(Al)II2c2 (Al-C only, no Mn-C) and (d) BCC-FeAlMnC-SS2SI2(Mn)II2c2 (Mn-C only, no Al-C).

Figure 12: C ordering on I sites ordering across the PMF I-site order-disorder transition temperature (from PMF calculations with 5 at.% C). The map displays (i) “2-sublattice”

ordering (i.e. type I1-I5 and other variants) (green), “3-sublattice” ordering (i.e. I1=I2=I3 and I4=I5=I6) (blue), the disordered solid solution (red) and other kind, less definite ordering (black) for interstitial C.

Figure 13: (a) C-C binding energy in bcc Fe for various neighbor range of the C-C pair, as obtained in the present work, and compared with earlier ab initio calculations [7]. Two kinds of fourth-neighbour pairs have to be distinguished, according to their being centered by an S site (labelled 4S) or by an I site (labelled 4I); (b) Influence of increasing *J(4S)* on C site occupancies (PMF).

BIBLIOGRAPHY

[1] ASM Handbook Volume 3: Alloy Phase Diagrams Editor: H. Okamoto, M. E. Schlesinger, E. M. Mueller, ASM International (2016).

[2] A. J. Bradley, A. H. Jay, The formation of superlattices in alloys of iron and aluminium, Proceedings of the Royal Society of London. Series A **136** (1932) 210-232. https://doi.org/10.1103/10.1098/rspa.1932.0075

[3] F. Stein, M. Palm, Re-determination of transition temperatures in the Fe–Al system by differential thermal analysis, International Journal of Materials Research **98** (2007) 580-588.
https://doi.org/10.3139/146.101512

[4] M. Wittmann, I. Baker, P. R. Munroe, The structure and mechanical properties of Fe_2AlMn single crystals, Philosophical Magazine **84** (2004) 3169-3194.
https://doi.org/10.1080/14786430410001716638

[5] Y. Liao, I. Baker, Study of yield stress anomaly of Fe_2MnAl single crystal by in situ TEM straining, Philosophical Magazine **92** (2012) 959-985.
https://doi.org/10.1080/14786435.2011.637983

[6] H. K. D. H. Bhadeshia, Carbon–Carbon Interactions in Iron, Journal of Materials Science **39** (2004) 3949-3955.
https://doi.org/10.1023/B:JMSC.0000031476.21217.fa

[7] C. Domain, C. S. Becquart, J. Foct, Ab initio study of foreign interstitial tom (C, N) interactions with intrinsic point defects in α-Fe, Physical Review B **69** (2004) 144112(16).
https://doi.org/10.1103/PhysRevB.69.144112

[8] C. Zener, Theory of strain interaction of solute atoms, Phys. Rev. 74 (1948) 639-647.
doi:10.1103/PhysRev.74.639.
[9] A.G. Khachaturyan, G.A. Shatalov, On the theory of the ordering of carbon atoms in a martensite crytal, Fiz. Met. Met. 32 (1971) 1-9.
[10] C.W. Sinclair, M. Perez, R.G.A. Veiga, A. Weck, Molecular dynamics study of the ordering of carbon in highly supersaturated alpha-Fe, Phys. Rev. B. 81 (2010) 224204.
doi:10.1103/PhysRevB.81.224204.
[11] N. Hatcher, G.K.H. Madsen, R. Drautz, DFT-based tight-binding modeling of iron-carbon, Phys. Rev. B. 86 (2012) 155115.
doi:10.1103/PhysRevB.86.155115.
[12] A. V. Ruban, Self-trapping of carbon atoms in alpha'-Fe during the martensitic transformation: A qualitative picture from ab initio calculations, Phys. Rev. B 90 (2014) 144106.
doi:10.1103/PhysRevB.90.144106.
[13] P. Maugis, F. Danoix, H. Zapolsky, S. Cazottes, M. Gouné, Temperature hysteresis of the order-disorder transition in carbon-supersaturated α-Fe, Phys. Rev. B. 96 (2017) 214104.
doi:10.1103/PhysRevB.96.214104.
[14] D. Kandaskalov, P. Maugis, Thermodynamic stabilities in the Fe−Fe16C2 system: Influence of carbon-carbon interactions studied by DFT, Comput. Mater. Sci. 150 (2018) 524-534.
doi:10.1016/j.commatsci.2018.04.025
[15] J.Y. Yan, A. V. Ruban, Configurational thermodynamics of C in body-centered cubic/tetragonal Fe: A combined computational study, Comput. Mater. Sci. 147 (2018) 293-303.
doi:10.1016/j.commatsci.2018.02.024.
[16] R. Besson, A. Legris, D. Connetable, P. Maugis, Atomic-scale study of low-temperature equilibria in iron-rich Al-C-Fe, Physical Review B **78** (2008) 014204(11).
https://doi.org/10.1103/PhysRevB.78.014204

[17] D. Connetable, J. Lacaze, P. Maugis, B. Sundman, A Calphad assessment of Al–C–Fe system with the κ carbide modelled as an ordered form of the fcc phase, Calphad **32** (2008) 361-370.
https://doi.org/10.1016/ j.calphad.2008.01.002
[18] A. T. Phan, M.-K. Paek, Y.-B. Kang, Phase Equilibria and Thermodynamics of the Fe–Al–C System: Critical Evaluation, Experiment and Thermodynamic Optimization, Acta Materialia **79** (2014) 1-15.
https://doi.org/10.1016/j.actamat.2014.07.006
[19] S. Chentouf, S. Cazottes, F. Danoix, M. Goune, H. Zapolsky, P. Maugis, Effect of interstitial carbon distribution and nickel substitution on the tetragonality of martensite: A first-principles study, Intermetallics. 89 (2017) 92-99.
doi:10.1016/j.intermet.2017.05.022.
[20] J. Sanchez, F. Ducastelle, D. Gratias, Generalized cluster description of multicomponent systems, Physica A: Statistical Mechanics and its Applications **128** (1984) 334-350.
https://doi.org/10.1016/0378-4371(84) 90096-7
[21] A. Finel, The Cluster Variation Method and Some Applications, Statics and Dynamics of Alloy Phase Transformations. Editors P. E. A. Turchi and A. Gonis. Boston, MA : Springer US, 1994.
https://doi.org/10.1007/978-1-4615-2476-2_33
[22] D. A. Contreras-Solorio, F. Mejia-Lira, J. L. Moran-Lopez, J. M. Sanchez, A study of the magnetic phases of BCC binary alloys, Journal de Physique Colloques **49** (1988) 105-106.
https://doi.org/10.1051/jphyscol:1988839
[23] G. Ceder, A derivation of the Ising model for the computation of phase diagrams, Computational Materials Science **1** (1993), 144-150.
https://doi.org/10.1016/0927-0256(93)90005-8
[24] D. le Bolloc'h, T. Cren, R. Caudron, A. Finel, Concentration variation of the effective pair interactions measured on the Pt-V system: Evaluation of the gamma expansion method, Computational Materials Science **8** (1997) 24-32.
https://doi.org/10.1016/S0927-0256(97)00012-8

[25] E. Clouet, J. M. Sanchez, C. Sigli, First-principles study of the solubility of Zr in Al, Physical Review B **65** (2002) 094105(13).
https://doi.org/10.1103/PhysRevB. 65.094105
[26] I. Toda-Caraballo, J. Wróbel, S. Dudarev, D. Nguyen-Manh, P. Rivera-Díaz-del-Castillo, Interatomic spacing distribution in multicomponent alloys, Acta Materialia **97** (2015) 156-169.
https://doi.org/10.1016/j.actamat.2015.07.010
[27] F. Schmid, K. Binder, Modelling Order-Disorder and Magnetic Transitions in Iron-Aluminium Alloys, Journal of Physics: Condensed Matter **4** (1992) 3569-3588.
https://doi.org/10.1088/0953-8984/4/13/019
[28] P. G. Gonzalez-Ormeno, H. M Petrilli, C. G. Schön, Ab initio calculation of the bcc Fe-Al phase diagram including magnetic interactions, Scripta. Mater. **54** (2006) 1271-1276.
[29] D. B. Laks, L. G. Ferreira, S. Froyen, A. Zunger, Efficient cluster expansion for substitutional systems, Physical Review B **46** (1992) 12587-12605.
https://doi.org/10.1103/PhysRevB.46.12587
[30] L. Holliger, R. Besson, Reciprocal-space cluster expansions for complex alloys with long-range interactions, Physical Review B **83** (2011) 174202(6).
https://doi.org/10.1103/PhysRevB.83.174202
[31] R. Besson, J. Kwon, L. Thuinet, M.-N. Avettand-Fènoël, A. Legris, First-principles study of Al-Cu energetics and consequences on athermal formation of Cu-rich compounds, Physical Review B **90** (2014) 214104(9).
https://doi.org/10.1103/PhysRevB.90.214104
[32] B. Sadigh, P. Erhart, A. Stukowski, A. Caro, Composition dependent interatomic potentials: A systematic approach to modelling multicomponent alloys, Philosophical Magazine **89** (2009) 3371-3391.
https://doi.org/10.1080/14786430903292373
[33] F. Ducastelle. Order and phase stability in alloys. North-Holland, 1991.
[34] V. Pierron-Bohnes, S. Lefebvre, M. Bessière, A. Finel, Short-range order in a single crystal of Fe-19.5 At.% Al in the ferromagnetic range measured through X-Ray diffuse scattering, Acta Metallurgica et Materialia **38** (1990) 2701-2710.
https://doi.org/10.1016/0956-7151(90)90284-N

[35] P. Hohenberg, W. Kohn, Inhomogeneous electron gas, Physical Review **136** (1964) 864-871.
https://doi.org/10.1103/PhysRev.136.B864
[36] W. Kohn, L. J. Sham, Self-consistent equations including exchange and correlation effects. Physical Review **140** (1965) 1133-1138.
https://doi.org/10.1103/PhysRev. 140.A1133
[37] J. W. D. Connolly, A. R. Williams, Density-functional theory applied to phase transformations in transition-metal alloys, Physical Review B **27** (1983) 5169-5172.
https://doi.org/10.1103/PhysRevB.27.5169
[38] A. van de Walle, G. Ceder, The effect of lattice vibrations on substitutional alloy Thermodynamics, Rev. Mod. Phys. 74 (2002) 11.
[39] G. Kresse, J. Hafner, Ab initio molecular dynamics for liquid metals, Phys. Rev. B **47 (**1993) 558–61.
[40] G. Kresse, D. Joubert, From ultrasoft pseudopotentials to the projector augmented-wave method, Phys. Rev. B **59 (**1999) 1758–75.
[41] J. P. Perdew, K. Burke, M. Ernzerhof, Generalized Gradient Approximation Made Simple, Phys. Rev. Lett. **77** (1996) 3865-3868.
https://doi.org/10.1103/PhysRevLett.77.3865
[42] J. P. Perdew, K. Burke, M. Ernzerhof, Generalized Gradient Approximation Made Simple, Phys. Rev. Lett. **78** (1997) 1396-1396.
https://doi.org/10.1103/PhysRevLett.78.1396
[43] D. Tingaud, R. Besson; Point defect phonons in intermetallics: $NiAl_3$ by atomic-scale simulation, Phys.Status Solidi C **6** (2009) 2008–2011.
[44] R. Besson, L. Thuinet, M.-A. Louchez, Atomic-scale study of stacking faults in Zr hydrides and implications on hydride formation, J. Phys. Condens. Matter **30** (2018) 315003(11).
[45] Madelung O 1978 Phonon–phonon interaction: thermal properties, *Introduction to Solid-State Theory* (Berlin: Springer) pp 314–26.
[46] C. Colinet, G. Inden, R. Kikuchi, CVM calculation of the phase diagram of b.c.c. Fe-Co-Al, Acat Metal. Mater. **41** (1993) 1109-1118.
[47] W. Schweika, Diffuse neutron scattering study of short-range order in Fe0.8Al0.2 alloy, Materials Research Society **166** (1989).

https://doi.org/10.1557/proc-166-249
[48] C. Bichara, G. Inden, Monte-Carlo calculation of the phase diagram of BCC Fe-Al alloys, Scripta Metallurgica et Materialia **25** (1991) 2607-2611.
https://doi.org/10.1016/0956-716X(91)90077-E
[49] V. Pierron-Bohnes, M. C. Cadeville, A. Finel, O. Schaerpf, Influence of magnetism on chemical order in a FeAl19.5 at% single crystal. high temperature measurements of neutron diffuse scattering, Journal de Physique I 1 (1991) 247-260.
https://doi.org/10.1051/jp1:1991128
[50] V. Pierron-Bohnes, M. C. Cadeville, A. Finel, R. Caudron, F. Solal, Pair interaction potentials deduced from neutron diffuse scattering in iron-based alloys, Physica B **180-181** (1992) 811-813.
https://doi.org/10.1016/0921-4526(92)90476-9
[51] L. Anthony, B. Fultz, Kinetics of B2, DO_3, and B32 ordering: results from pair approximation calculations and Monte-Carlo simulations, Journal of Materials Research **9** (1994), 348-356.
https://doi.org/10.1557/JMR.1994.0348
[52] P. Dey, R. Nazarov, B. Dutta, M. Yao, M. Herbig, M. Friák, T. Hickel, D. Raabe, J. Neugebauer, Ab initio explanation of disorder and off-Stoichiometry in Fe-Mn-Al-C κ Carbides, Physical Review B **95** (2017) 104108(14).
https://doi.org/10.1103/PhysRevB.95.104108
[53] J.-P. Landesman, G. Treglia, P. Turchi, F. Ducastelle, Electronic structure and pairwise interactions in substoichiometric transition metal carbides and nitrides, J. Phys. **46** (1985) 1001-1015.
https://doi.org/10.1051/jphys:019850046060100100
[54] A. Finel, Contribution à l'étude des effets d'ordre dans le cadre du modèle d'Ising : états de base et diagrammes de phase, Thèse de doctorat (1987). http://www.theses.fr/1987PA066372.
[55] M. Zelený, M. Friák, M. Šob, Ab initio study of energetics and magnetism of Fe, Co, and Ni along the trigonal deformation path, Physical Review B **83** (2011) 184424(7).
doi : 10.1103/PhysRevB. 83.184424.

[56] M. Friák, T. Hickel, F. Körmann, A. Udyansky, A. Dick, J. von Pezold, D. Ma, O. Kim, W. Counts, M. Šob, T. Gebhardt, D. Music, J. Schneider, D. Raabe, J. Neugebauer, Determining the elasticity of materials employing quantum mechanical approaches: from the electronic ground state to the limits of materials stability, Steel Research International **82** (2011) 86-100.
doi : 10.1002/srin.201000264.
[57] N. I. Medvedeva, D. V. Aken, J. E. Medvedeva, Magnetism in bcc and fcc Fe with carbon and manganese, Journal of Physics: Condensed Matter **22** (2010) 316002(7).
[58] C. Varvenne, F. Bruneval, M.-C. Marinica, E. Clouet, Point defect modeling in materials: Coupling ab initio and elasticity approaches, Physical Review B **88** (2013).
doi : 10.1103/PhysRevB.88.134102.

APPENDIX

Point Mean Field for A-B-C-D alloys

with A-B-C on substitutional (S) sites and D on interstitial (I) sites

In the general formulation, we consider an ensemble of S and I sites occupied by chemical species, the indexes for sites and species being respectively n and i. The site occupancy variables p_n^i are defined such as $p_n^i = 1$ if site n is occupied by species i, $p_n^i = 0$ otherwise. The basic PMF approximation consists in assuming that the density matrix can be written as a product over sites $\rho = \prod_n \rho_n$ with $\rho_n = \sum_i \langle p_n^i \rangle p_n^i$. This approximation readily allows to obtain expressions, as functions of the site variables $\langle p_n^i \rangle \widehat{=} c_n^i$, for the entropy as well as for statistical averages of useful quantities such as the site occupancy products $p_n^i p_m^j$ appearing in the Hamiltonian. Moreover, while all these site variables c_n^i can in principle be regarded as independent, tractability of the PFM formalism requires to group them into classes with equal values, i.e. to define several sublattices. For instance, in the present case of S-site bcc alloy, the well-known decomposition into four sublattices S∈{α, β, γ, δ} was used, hence $c_n^i = c_S^i$ for all sites n belonging to sublattice S. A similar assumption was used for I sites, leading to a set of six I sublattices.

The PMF is best formulated in grand canonical form, adding to the Hamiltonian a chemical potential term proportional to the amounts of chemical species. The linear term of the Hamiltonian is thus:

$$\langle H_1 - N_i \mu_i \rangle_{PMF} = \sum_S \{[J_1^B - \mu^B + \mu^A] N_S c_S^B + [J_1^C - \mu^C + \mu^A] N_S c_S^C\} + \sum_I [J_1^D - \mu^D]\, N_I c_I^D$$

with N_S the number of sites of type S in the system. The sums run over the various types of S and I sublattices.

For interactions between S sites, the B-B pair part of the PMF hamiltonian is:

$$\langle H_2^{BB} \rangle_{PMF} = \frac{1}{2} \sum_q J_{qN}^{BB} \sum_{S,S'} N_S z_{S'(S)}^{qN}\, c_S^B c_{S'}^B$$

with $z_{S'(S)}^{qN}$ the number of S' neighbor sites in the q[th] neighbor shell of a given S site. The $\langle H_2^{CC}\rangle_{PMF}$ part is written along the same lines, and:

$$\langle H_2^{BC}\rangle_{PMF} = \sum_q J_{qN}^{BC} \sum_{S,S'} N_S z_{S'(S)}^{qN} c_S^B c_{S'}^C$$

For interactions between S and I sites, the pair hamiltonian is:

$$\langle H_2^{BD}\rangle_{PMF} = \sum_q J_{qN}^{BD} \sum_{S,I} N_S z_{I(S)}^{qN} c_S^B c_I^D$$

and similarly for $\langle H_2^{CD}\rangle_{PMF}$.

Finally, for interactions between I sites:

$$\langle H_2^{DD}\rangle_{PMF} = \frac{1}{2}\sum_q J_{qN}^{DD} \sum_{I,I'} N_{I'} z_{I'(I)}^{qN} c_I^D c_{I'}^D$$

From the PMF approximation, the entropy is:

$$\frac{-S_{PMF}}{k} = \sum_S N_S[c_S^B \ln c_S^B + c_S^B \ln c_S^B + (1 - c_S^B - c_S^C)\ln(1 - c_S^B - c_S^C)] + \sum_I N_I[c_I^D \ln c_I^D + (1 - c_I^D)\ln(1 - c_I^D)]$$

The PMF free energy functional is thus:

$$F_{PMF} = \langle H_2^{BB}\rangle_{PMF} + \langle H_2^{BC}\rangle_{PMF} + \langle H_2^{CC}\rangle_{PMF} + \langle H_2^{BD}\rangle_{PMF} + \langle H_2^{CD}\rangle_{PMF} + \langle H_2^{DD}\rangle_{PMF} + \langle H_1 - N_i\mu_i\rangle_{PMF} - TS_{PMF}$$

Minimizing this functional with respect to the PMF variables $\{c_S^B, c_S^C, c_I^D\}$ yields an implicit equation for each $S_0 \in S$:

$$\sum_q \sum_S z_{S(S_0)}^{qN}\left[J_{qN}^{BB} c_S^B + J_{qN}^{BC} c_S^C\right] + \sum_q \sum_I z_{I(S_0)}^{qN} J_{qN}^{BD} c_I^D + J_1^B - \mu^B + \mu^A + kT\ln\frac{c_{S_0}^B}{1 - c_{S_0}^B - c_{S_0}^C} = 0$$

also written as :

$$G^B_{S_0}(\{c^B_S, c^C_S, c^D_I\}) + kT\ln\frac{c^B_{S_0}}{1 - c^B_{S_0} - c^C_{S_0}} = 0$$

which can be inverted to yield :

$$c^B_{S_0} = \frac{X^B_{S_0}}{1 + X^B_{S_0} + X^C_{S_0}}$$

with $X^B_{S_0}(\{c^B_S, c^C_S, c^D_I\}) \widehat{=} e^{-G^B_{S_0}/kT}$. Similar expressions hold for c^C_S.

Implicit equations for c^D_I are obtained for each $I_0 \in I$ as:

$$\sum_q \sum_S z^{qN}_{S(I_0)} \left[J^{BD}_{qN} c^B_S + J^{CD}_{qN} c^C_S\right] + \sum_q \sum_I z^{qN}_{I(I_0)} J^{DD}_{qN} c^D_I + J^D_1 - \mu^D + kT\ln\frac{c^D_{I_0}}{1 - c^D_{I_0}} = 0$$

which can be written as:

$$G^D_{I_0}(\{c^B_S, c^C_S, c^D_I\}) + kT\ln\frac{c^D_{I_0}}{1 - c^D_{I_0}} = 0$$

and inverted to yield :

$$c^D_{I_0} = \frac{X^D_{I_0}}{1+X^D_{I_0}} \text{ with } X^D_{I_0}(\{c^B_S, c^C_S, c^D_I\}) = e^{-G^D_{I_0}/kT}$$

The composition constraint on D is :

$$\sum_I N_I\, c^D_I = \frac{x_D}{1 - x_D} \sum_S N_S$$

with x_D the imposed D atomic fraction. The μ^D chemical potential thus becomes an additional variable which has to be handled the same way as the PFM set $\{c^B_S, c^C_S, c^D_I\}$.

Figure 1

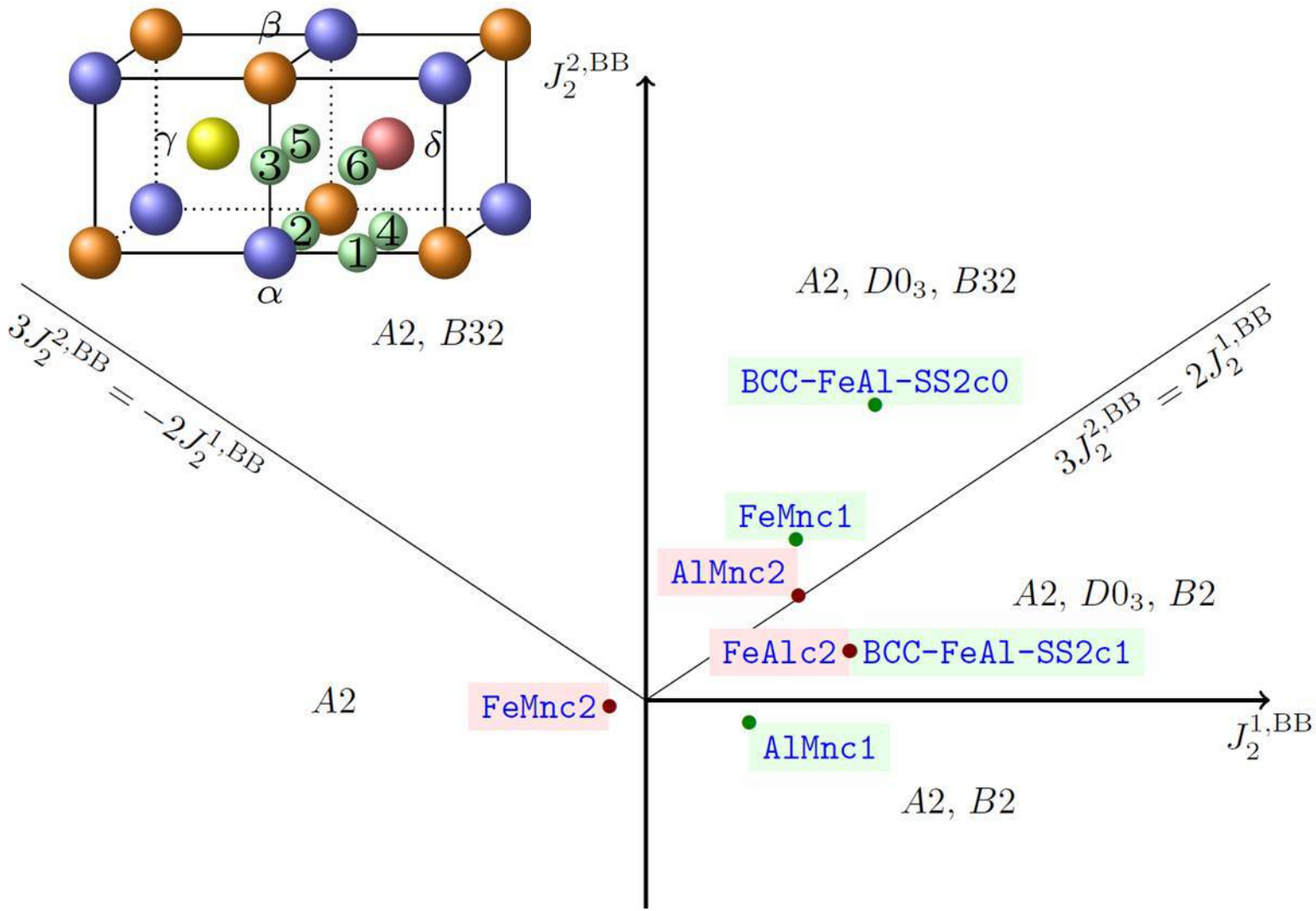
β
γ
δ
α
1
2
3
4
5
6
$J_2^{2,\mathrm{BB}}$
$J_2^{1,\mathrm{BB}}$
$3J_2^{2,\mathrm{BB}} = -2J_2^{1,\mathrm{BB}}$
$3J_2^{2,\mathrm{BB}} = 2J_2^{1,\mathrm{BB}}$
A2, B32
A2, D0$_3$, B32
A2, D0$_3$, B2
A2, B2
A2
BCC-FeAl-SS2c0
FeMnc1
AlMnc2
FeAlc2
BCC-FeAl-SS2c1
FeMnc2
AlMnc1

Figure 2

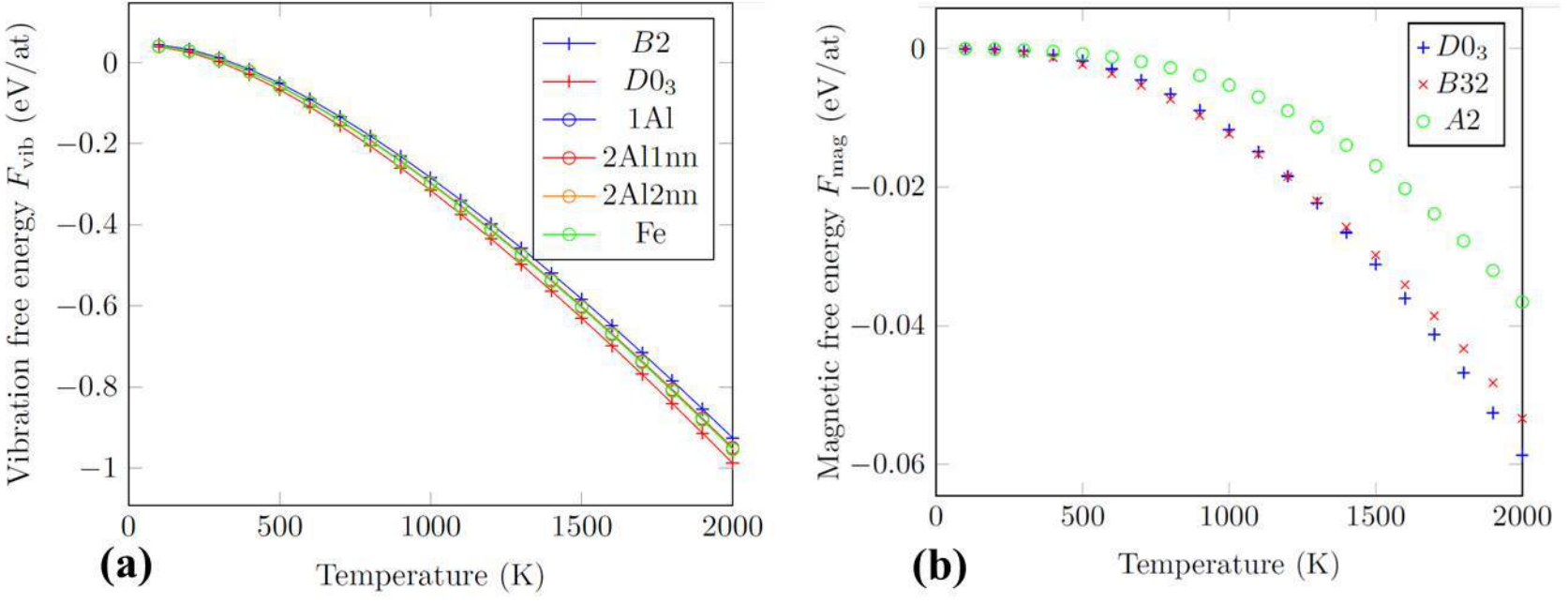
Vibration free energy F_{vib} (eV/at)
0
−0.2
−0.4
−0.6
−0.8
−1
0
500
1000
1500
2000
Temperature (K)
$B2$
$D0_3$
1Al
2Al1nn
2Al2nn
Fe
(a)
Magnetic free energy F_{mag} (eV/at)
0
−0.02
−0.04
−0.06
0
500
1000
1500
2000
Temperature (K)
$D0_3$
$B32$
$A2$
(b)

Figure 3

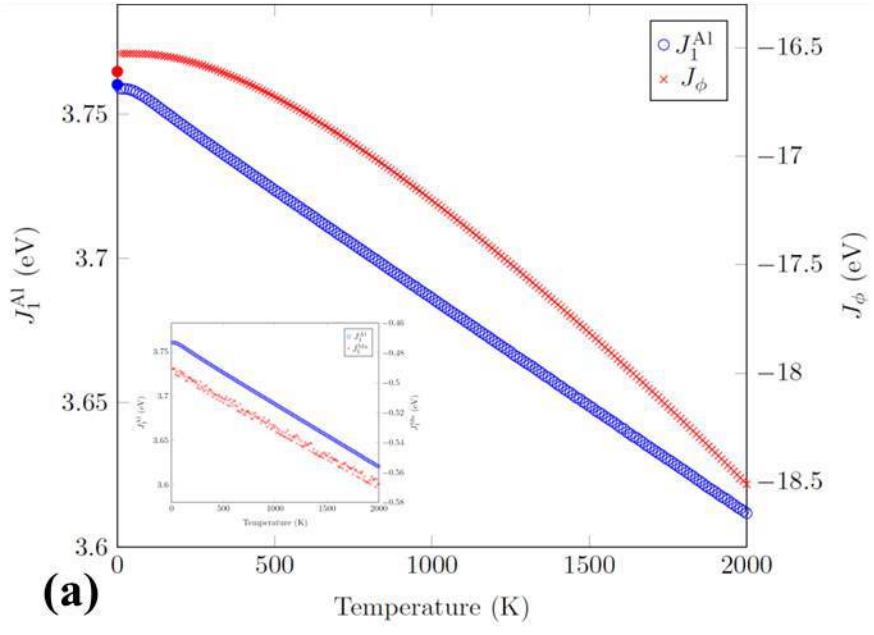
J_1^{Al}
J_ϕ
J_1^{Al} (eV)
J_ϕ (eV)
Temperature (K)
(a)

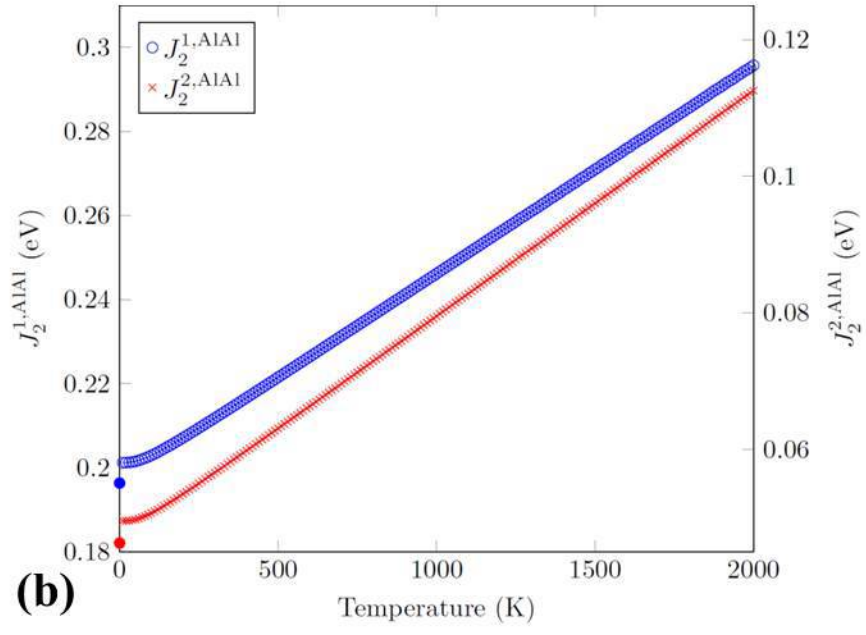
$J_2^{1,\mathrm{AlAl}}$
$J_2^{2,\mathrm{AlAl}}$
$J_2^{1,\mathrm{AlAl}}$ (eV)
$J_2^{2,\mathrm{AlAl}}$ (eV)
Temperature (K)
(b)

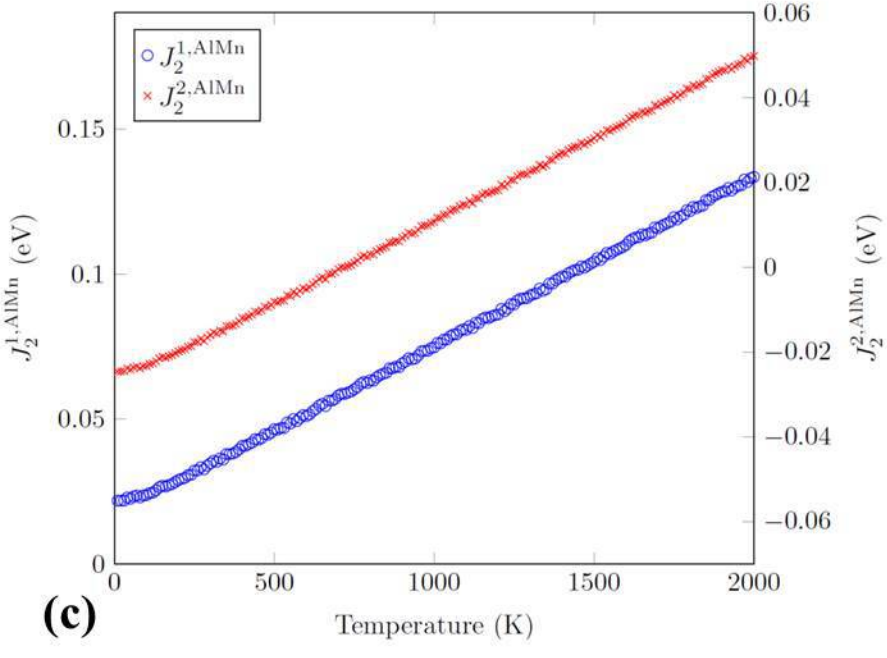
$J_2^{1,\mathrm{AlMn}}$
$J_2^{2,\mathrm{AlMn}}$
$J_2^{1,\mathrm{AlMn}}$ (eV)
$J_2^{2,\mathrm{AlMn}}$ (eV)
Temperature (K)
(c)

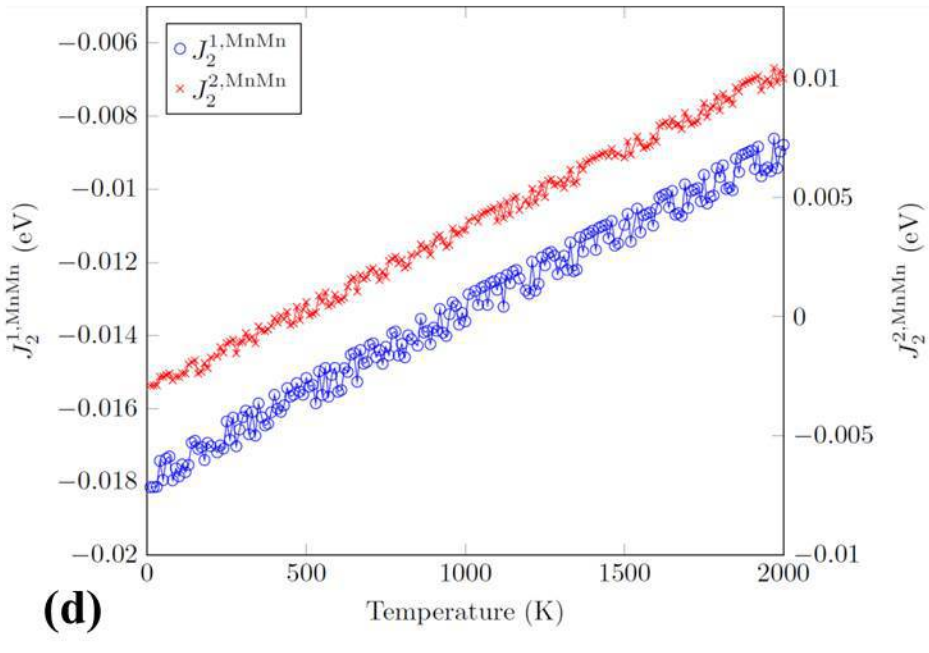
$J_2^{1,\mathrm{MnMn}}$
$J_2^{2,\mathrm{MnMn}}$
$J_2^{1,\mathrm{MnMn}}$ (eV)
$J_2^{2,\mathrm{MnMn}}$ (eV)
Temperature (K)
(d)

Figure 4

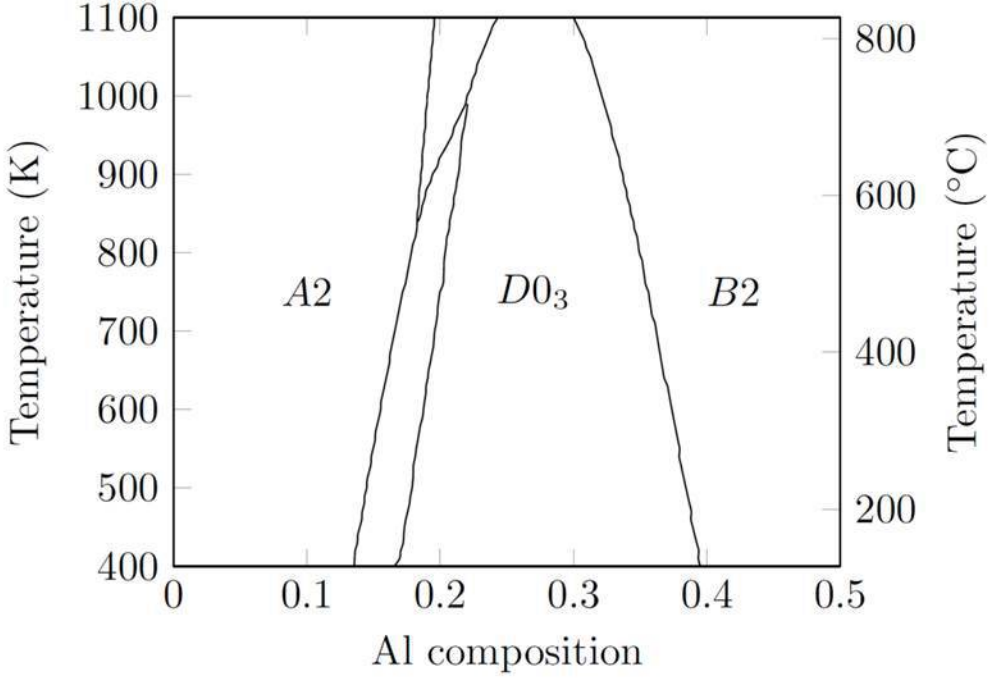

(a) CVM - BCC-FeAl-SS2c1T

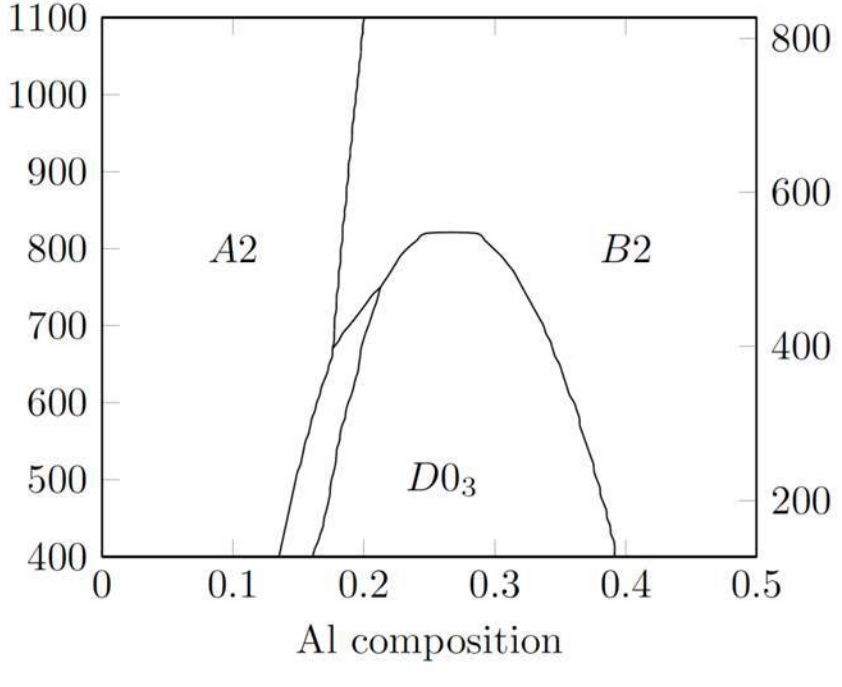

(b) CVM - BCC-FeAl-SS2c1T390

Figure 5

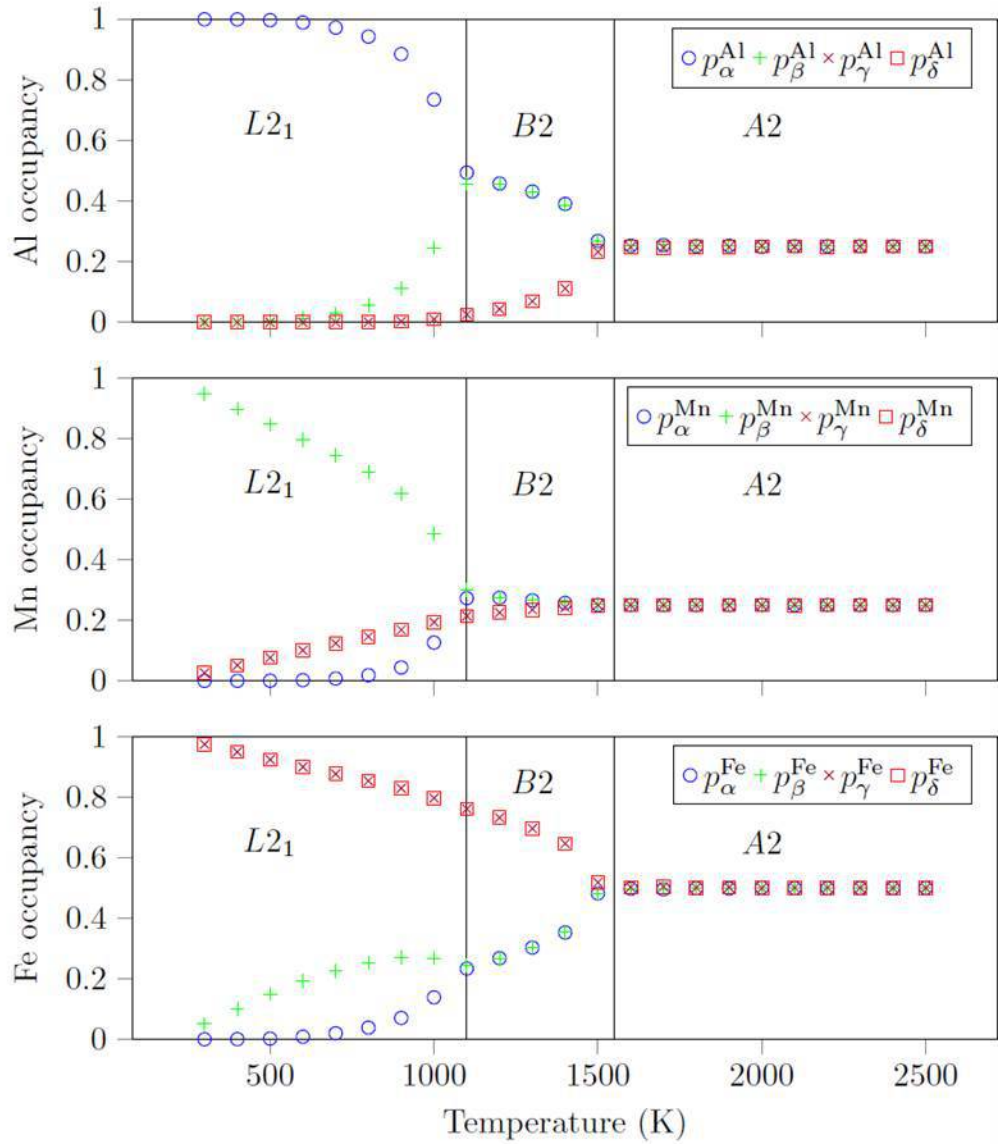
Al occupancy
Mn occupancy
Fe occupancy
$L2_1$
$B2$
$A2$
p_α^{Al} p_β^{Al} p_γ^{Al} p_δ^{Al}
p_α^{Mn} p_β^{Mn} p_γ^{Mn} p_δ^{Mn}
p_α^{Fe} p_β^{Fe} p_γ^{Fe} p_δ^{Fe}
0
0.2
0.4
0.6
0.8
1
500
1000
1500
2000
2500
Temperature (K)

Figure 6

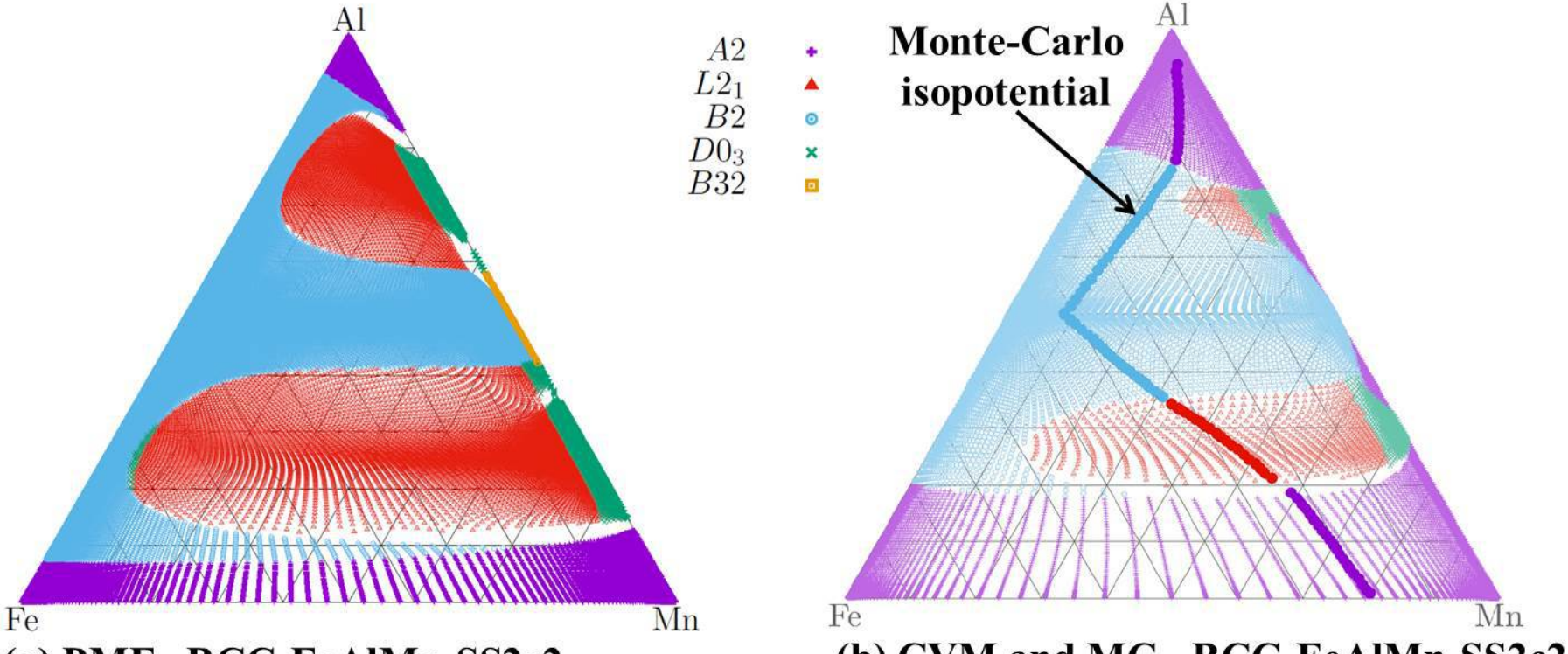

(a) PMF - BCC-FeAlMn-SS2c2

(b) CVM and MC - BCC-FeAlMn-SS2c2

Figure 7

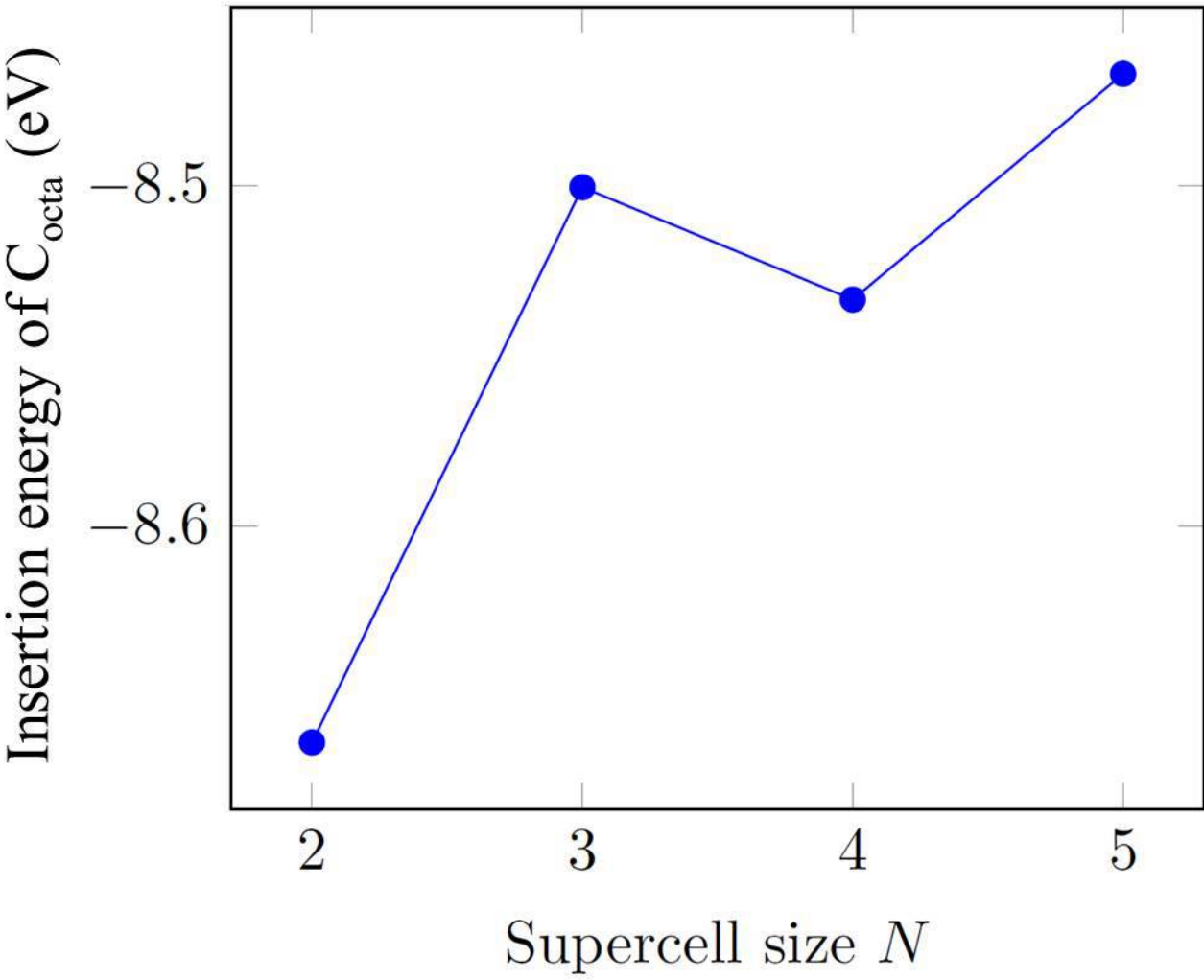

Figure 8

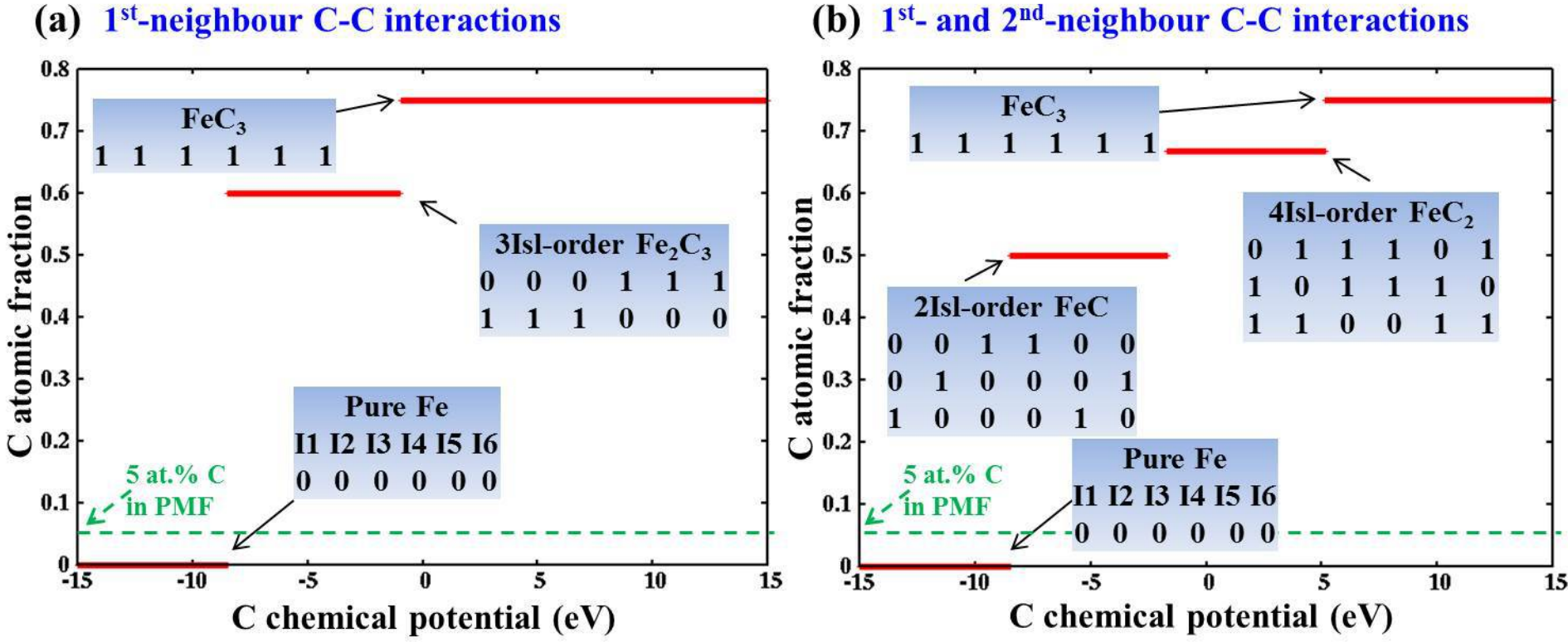
(a) 1st-neighbour C-C interactions
(b) 1st- and 2nd-neighbour C-C interactions
C atomic fraction
C chemical potential (eV)
FeC3
1 1 1 1 1 1
3Isl-order Fe2C3
0 0 0 1 1 1
1 1 1 0 0 0
Pure Fe
I1 I2 I3 I4 I5 I6
0 0 0 0 0 0
5 at.% C in PMF
2Isl-order FeC
0 0 1 1 0 0
0 1 0 0 0 1
1 0 0 0 1 0
4Isl-order FeC2
0 1 1 1 0 1
1 0 1 1 1 0
1 1 0 0 1 1

Figure 9

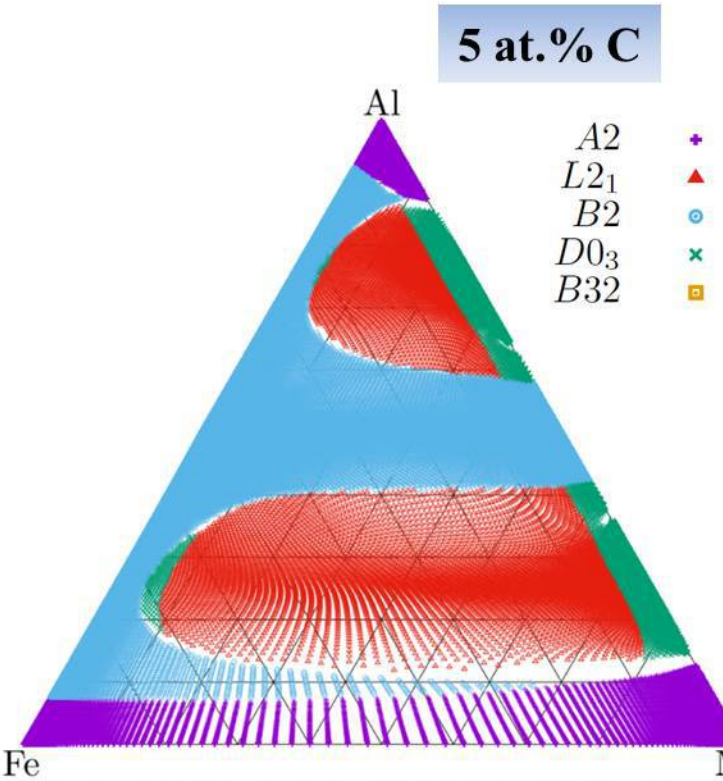

(a) BCC-FeAlMnC-SS2SI2c2 - S ordering

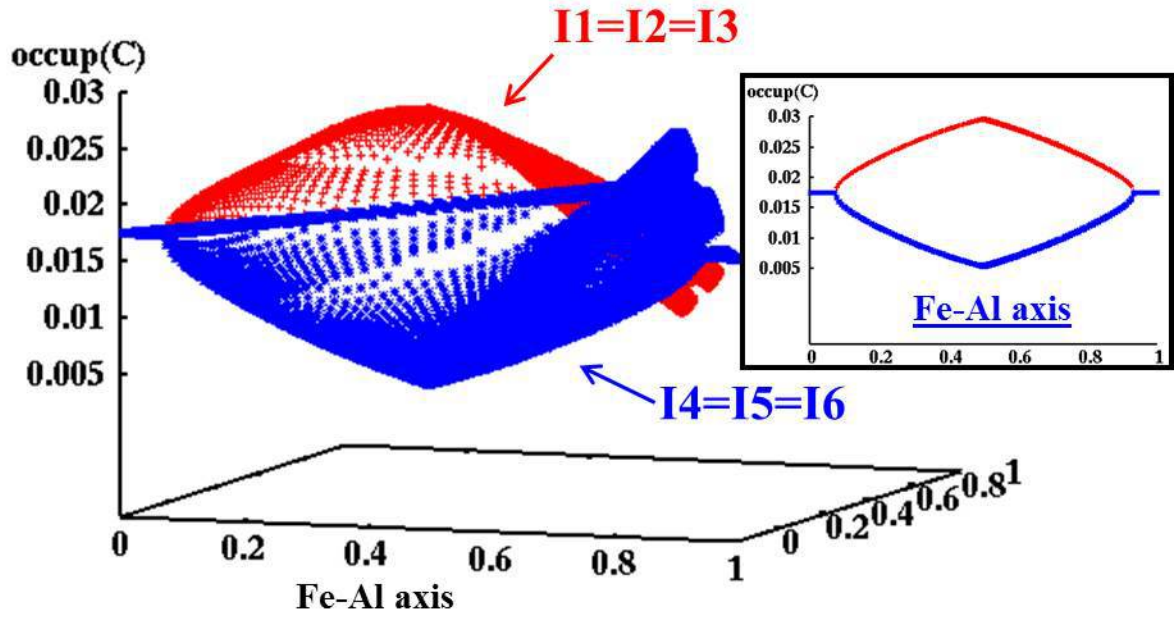

(b) BCC-FeAlMnC-SS2SI2c2 - I ordering

Figure 10

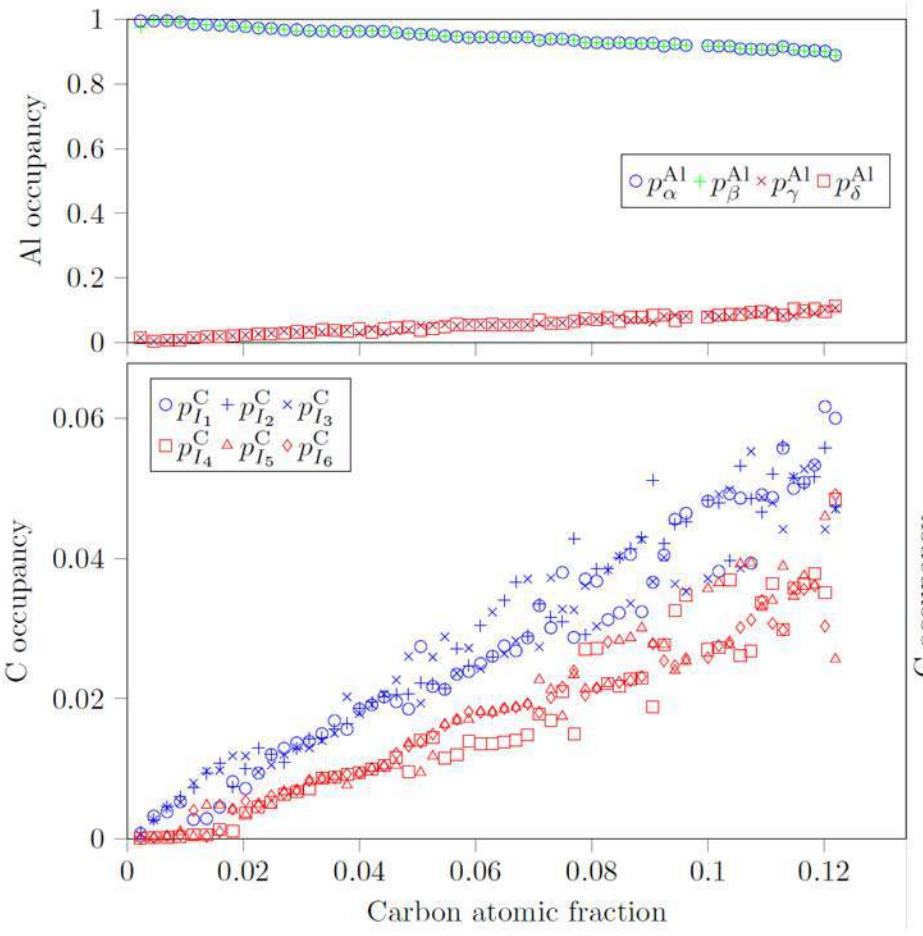

(a) B2-FeAlC$_x$ - BCC-FeAlMnC-SS2SI2c2

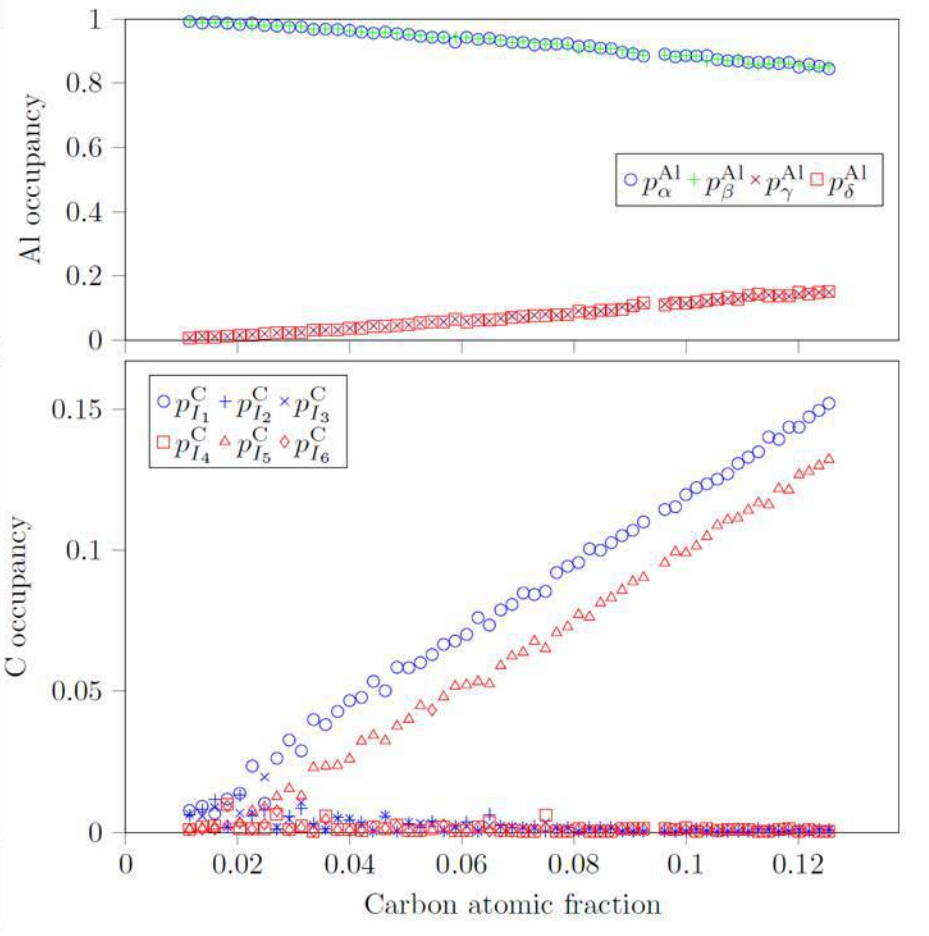

(b) B2-FeAlC$_x$ - BCC-FeAlMnC-SS2SI2II2c2

Figure 11

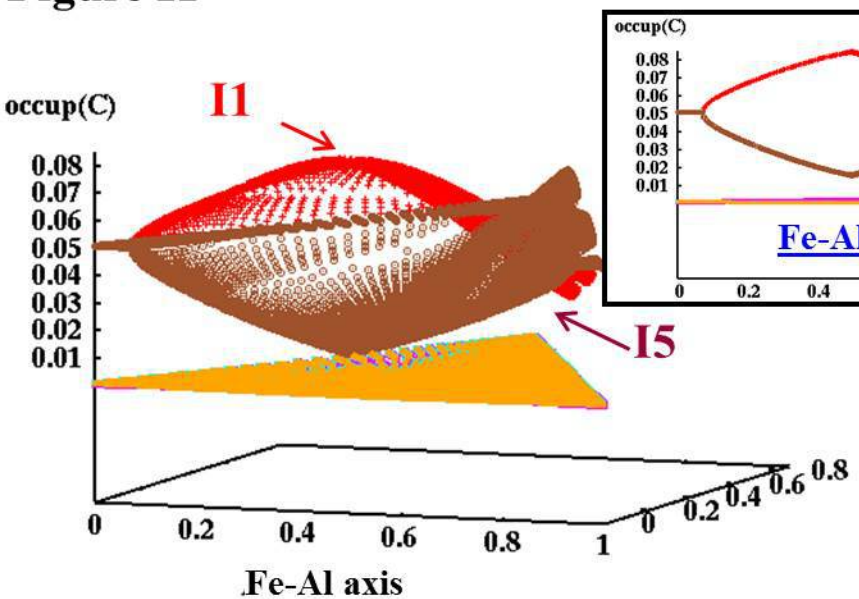

(a) BCC-FeAlMnC-SS2SI2II2c2

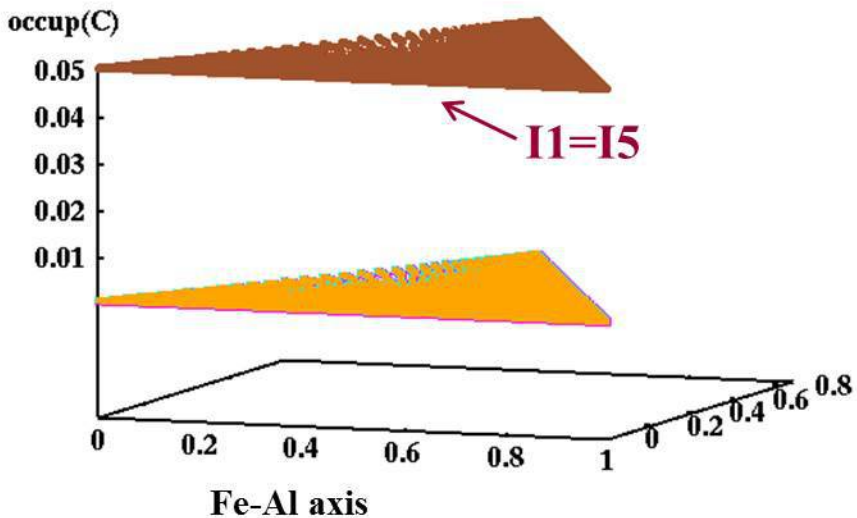

(b) BCC-FeAlMnC-SS2SI0II2c2
(no Al-C, no Mn-C)

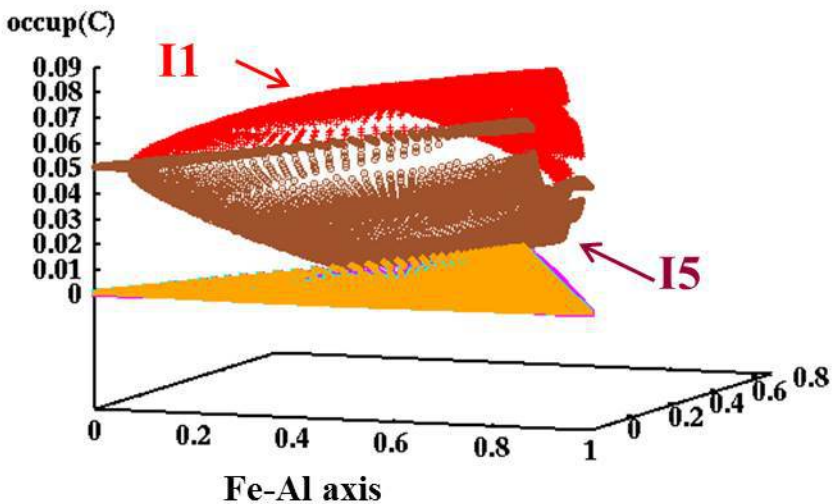

(c) BCC-FeAlMnC-SS2SI2(Al)II2c2
(Al-C only, no Mn-C)

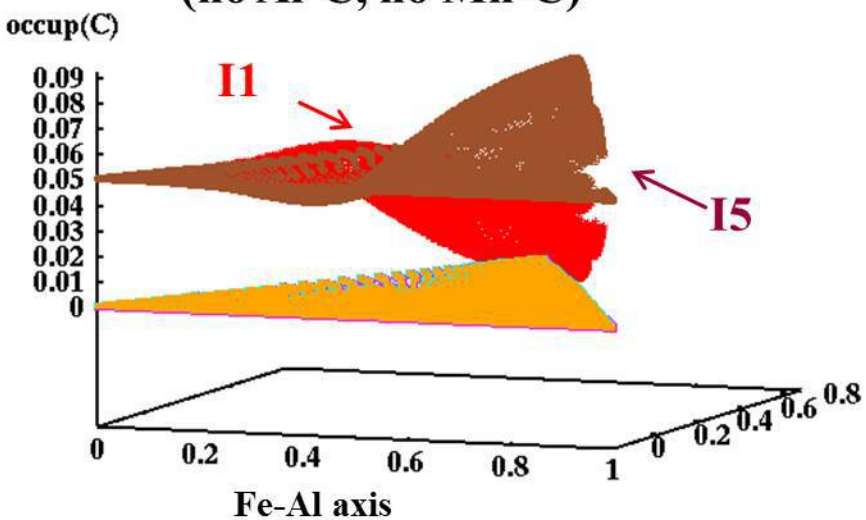

(d) BCC-FeAlMnC-SS2SI2(Mn)II2c2
(Mn-C only, no Al-C)

Figure 12

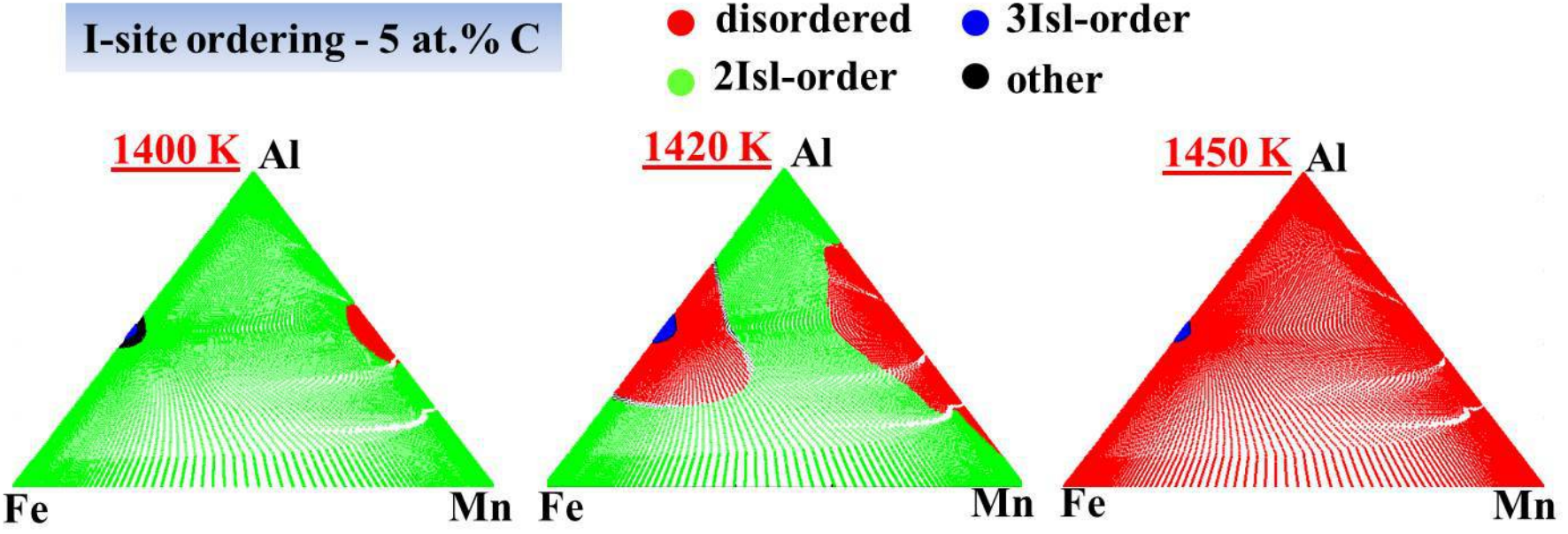
I-site ordering - 5 at.% C
disordered
3Isl-order
2Isl-order
other
1400 K
Al
Fe
Mn
1420 K
Al
Fe
Mn
1450 K
Al
Fe
Mn

Figure 13

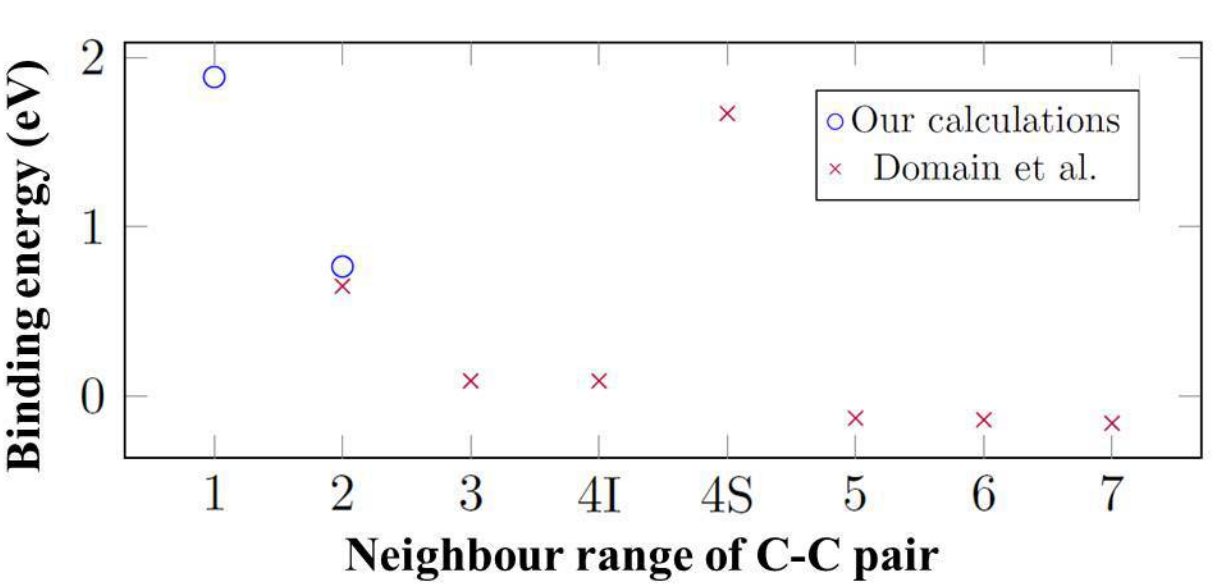
(a)
Binding energy (eV)
2
1
0
Our calculations
Domain et al.
1
2
3
4I
4S
5
6
7
Neighbour range of C-C pair

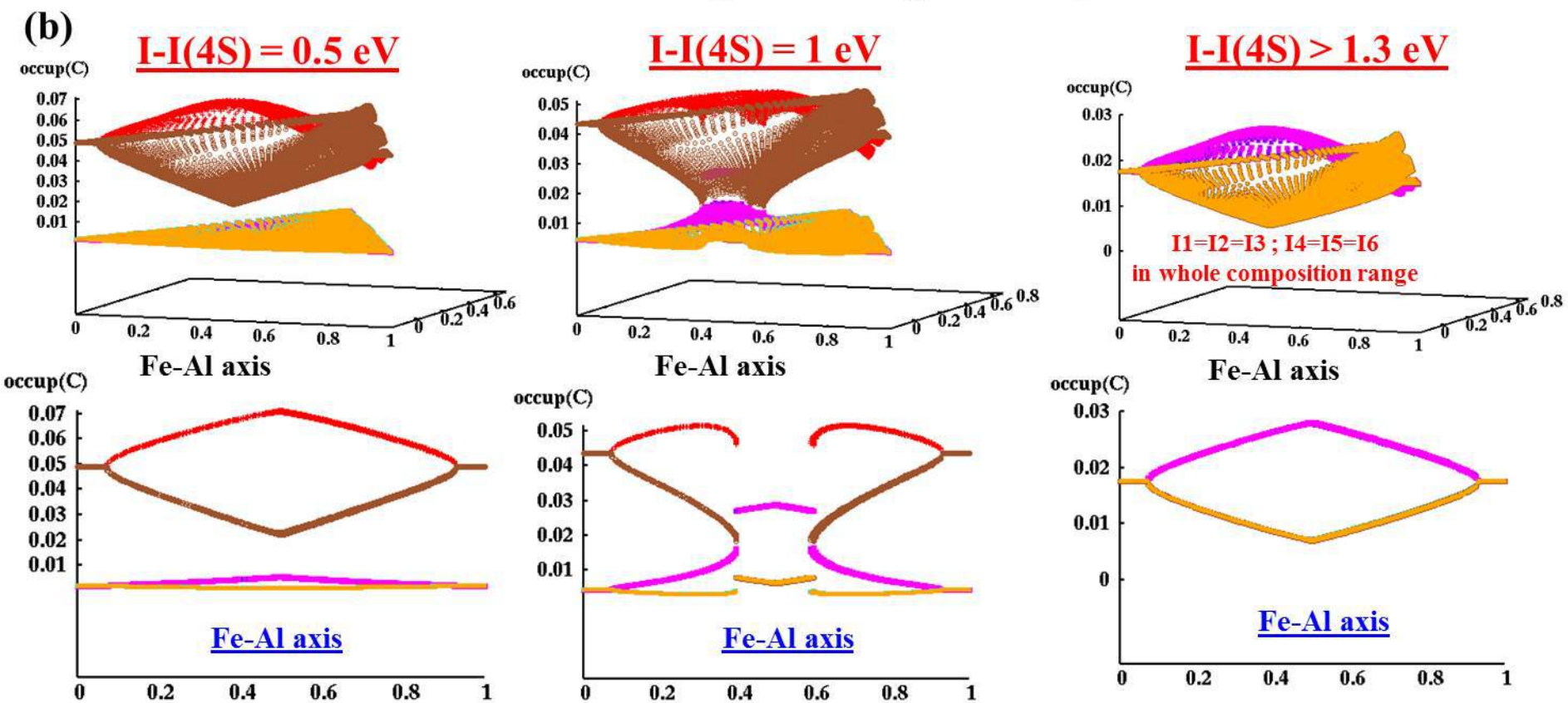
(b)
I-I(4S) = 0.5 eV
I-I(4S) = 1 eV
I-I(4S) > 1.3 eV
occup(C)
Fe-Al axis
I1=I2=I3 ; I4=I5=I6
in whole composition range

Selection of ab initio input database

Atomic-scale cluster expansion modelling

Statistical thermodynamics

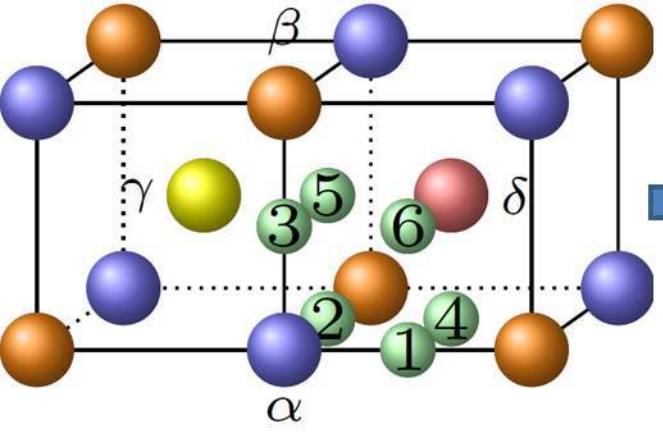

Unit cell for Al- and Mn-doped ferritic steels

$$H = \sum_{\alpha} J_{\alpha}\sigma_{\alpha}$$

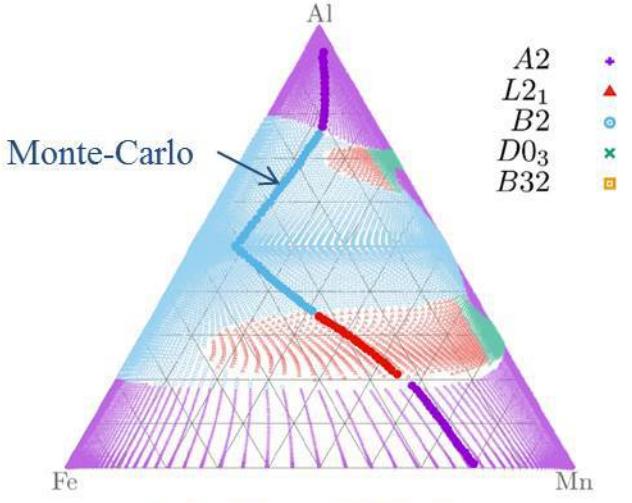

Point Mean-Field phase diagram of Fe-Al-Mn

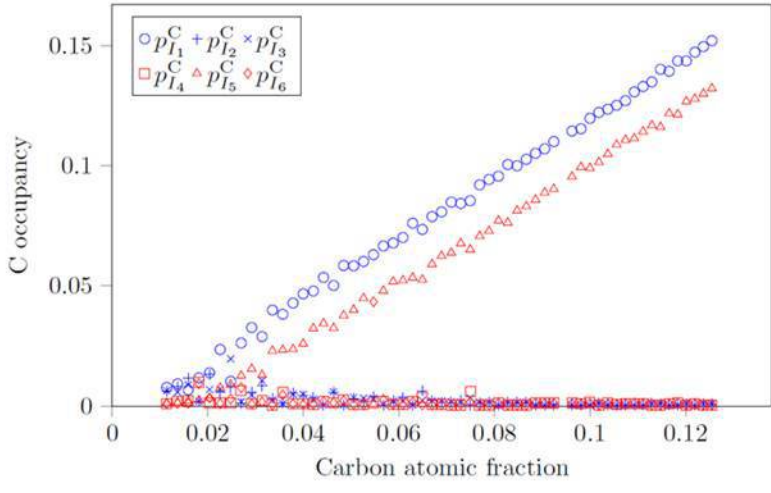

Carbon ordering on interstitial sites